

2017

Morphological and Geochemical Characteristics of Volcanic Ash: Insights into Eruption Energetics

Megan Grace Clark
Lehigh University

Follow this and additional works at: <http://preserve.lehigh.edu/etd>



Part of the [Environmental Sciences Commons](#)

Recommended Citation

Clark, Megan Grace, "Morphological and Geochemical Characteristics of Volcanic Ash: Insights into Eruption Energetics" (2017).
Theses and Dissertations. 2555.
<http://preserve.lehigh.edu/etd/2555>

This Thesis is brought to you for free and open access by Lehigh Preserve. It has been accepted for inclusion in Theses and Dissertations by an authorized administrator of Lehigh Preserve. For more information, please contact preserve@lehigh.edu.

Morphological and Geochemical Characteristics of Volcanic Ash: Insights into
Eruption Energetics

By
Megan G Clark

A Thesis
Presented to the Graduate and Research Committee
of Lehigh University
in Candidacy for the Degree of
Master of Science

in
Earth and Environmental Sciences

Lehigh University

May 2017

© 2017 Copyright

Megan Clark

Thesis is accepted and approved in partial fulfillment of the requirements for the
Master of Science in Earth and Environmental Sciences

Morphological and Geochemical Characteristics of Volcanic Ash: Insights into
Eruption Energetics

Megan G. Clark

Date Approved

Dork L. Sahagian
(Advisor)

Kenneth P. Kodama
(Committee Member)

Gray E. Bebout
(Committee Member)

David J. Anastasio
(Department Chair)

ACKNOWLEDGEMENTS

I would like to thank Dork Sahagian for his invaluable guidance on this project and in my professional development. Without Dork, this project would not have been possible, and I am forever grateful for his role in, not only this study, but also my development as a scientist and professional. I would also like to thank Ken Kodama and Gray Bebout for their thoughtful insight on this project as my committee members.

I would also like to thank Kim Genareau at the University of Alabama for providing all of the ash samples used in this study. I also thank Bruce Idleman for his invaluable assistance with the SEM and Tetyana Ignatova and Slava Rotkin from Lehigh University's Physics Department for their support on the Micro Raman. I also would like to thank Candace Wygel for her thorough proofreading, and for being a great "little sister."

I would like to acknowledge funding from the Department of Earth and Environmental Sciences, without which none of this would have been possible.

I have made some truly amazing friends here at Lehigh. There are far too many to list, but I want to acknowledge all the EES faculty, staff, and students who have been an integral part of my success. I am truly grateful to all of you for your friendship and camaraderie. I would also like to thank my friends and family, both here and elsewhere, for their support throughout my career. Lastly, thanks to my boyfriend, Dylan, and dog, Gus for the love, encouragement, and productive conversation about this work.

TABLE OF CONTENTS

Title Page.....	i
Copyright Page.....	ii
Approval Page.....	iii
Acknowledgements.....	iv
Table of Contents.....	v
List of Tables.....	vi
List of Figures.....	vii
Abstract.....	1
Introduction.....	3
Background.....	4
Scope and Implications.....	14
Goals and Hypotheses.....	21
Geologic Setting.....	24
Methods.....	26
Results.....	31
Discussion.....	39
Conclusions.....	59
Recommendations for Future Research.....	61
References.....	65
Appendices.....	70
Vita.....	96

LIST OF TABLES

Table 1: Summary of eruptive characteristics of eruptions examined in this study.....	25
Appendix 1: Raw ash morphology data and SE ratings obtained from SEM observation.....	70

LIST OF FIGURES

- Figure 1:** Conceptual model of conduit processes. The initial stages involve bubble nucleation at depth and volatile diffusion to pre-existing bubbles. With relatively slow decompression (left side), volatiles diffuse into these bubbles throughout the history of magma ascent and decompression, and only one size population of bubbles is observed in erupted products. With relatively rapid decompression (right side), volatiles do not have sufficient time to diffuse into pre-existing bubbles, so magma becomes sufficiently oversaturated to nucleate a second phase of bubbles, which are very small and numerous. These are termed syn-eruptive bubbles. With extreme eruption rates, volatiles may remain in the melt upon fragmentation and quenching..... 5
- Figure 2:** Schematic diagram of magma rising through the conduit and reaching the point of fragmentation. 1. Initial bubble nucleation with volatiles remaining in the melt, 2. Bubbles grow via diffusion of volatiles out of the melt and decompression, 3a. Magmatic foam consisting of large, growing bubbles with thin walls of viscous magma in between them, 3b. Magma fragmentation due to tensile stresses exceeding tensile strength of the magma, 3b. Resulting gassy spray consisting of fragmented bubble walls entrained in a high energy gas. Adapted from Sahagian (1999)..... 6
- Figure 3:** Schematic diagram illustrating the scope of this study. I seek to establish the relationship between ash morphology and eruption energetics. This could allow for ash collected from an eruption to be analyzed and used to better characterize the explosivity of the eruption from which it came.....15
- Figure 4:** Predicted relationship between decompression rate (represented by VEI) and SE Rating (the percent of examined particles that display syn-eruptive bubbles). The SE rating is expected to increase with increasing decompression rate, and thus increasing explosivity of the eruptive style..... 23
- Figure 5:** Summary of results from the ash morphology portion of this study. The table is plotted in the chart. Data shows a clear threshold of decompression rates below VEI 4, and gradual scaling of increasing SE rating with decompression rate for eruptions VEI 4-6. Error was calculated using percent of particles I was even slightly unsure about in my classification. Classification parameters were kept consistent throughout analysis; therefore, likelihood that SE Ratings fall elsewhere besides plotted points is very low..... 32
- Figure 6 (a-f):** SEM images of ash representative ash particles from all eruptions. (a) Novarupta-Katmai, (b) Saint Helens, and (c) Augustine clearly display syn-eruptive and pre-eruptive bubbles, with syn-eruptive bubbles being extremely abundant and closely spaced in the majority of the particles that were examined. (d) Okmok and (e) Spurr also clearly display syn-eruptive and pre-eruptive

bubbles, with syn-eruptive bubbles being slightly less abundant and spaced farther apart in the majority of examined particles. **(f)** Redoubt does not display syn-eruptive bubbles, only large, pre-eruptive bubble walls are visible in the majority of examined particles..... 33

Figure 7 (a-b): Representative Micro Raman Spectra. Peek for water species is represented by the blue arrow. Further explanation of spectra can be found in **Section 8.2.1.** **(a)** Okmok spectra. **(b)** Spurr spectra..... 37

Figure 8: Conceptual diagram of the volcanic conduit during magmatic ascent (vertical direction of magmatic movement indicated by gray arrows). Ascent velocities are highest at the conduit axis and lowest at the walls (indicated by black arrows). Red stretched lines near walls are indicative of likely regions of shear due to the horizontal velocity gradient. The bottom plot shows velocity changes across the conduit, with the steepest velocity gradient occurring near the walls and little to no velocity gradient in the center..... 46

Figure 9 (a-c): SEM images showing sheared particles. **(a)** Katmai. **(b)** Saint Helens. **(c)** Augustine..... 48

Figure 10: Generalized plot of time versus ascent velocity for magmas of various compositions. Andesite, because of higher diffusivity, has greater bubble growth and depth, allowing for fairly fast ascent velocities at depth, but a volatile-depleted melt upon eruption, causing little late-stage increase in velocity and ultimately slower final ascent velocities and eruption rates. Conversely, rhyolite, because of lower diffusivity, has less bubble growth at depth, allowing for fairly slow ascent velocities at depth, but great supersaturation upon eruption, causing a large late-stage increase in velocity and ultimately faster ascent velocities and eruption rates..... 53

Appendix 2: Particle size distributions from each eruption, differentiating between particles with syn-eruptive bubbles (SE) and particles with no syn-eruptive bubbles (No SE). There is not clear correlation between particle size and the likelihood of preserving or not preserving syn-eruptive bubbles..... 93

ABSTRACT

Energetic volcanic eruptions are driven by early bubble nucleation. In some cases, during magmatic ascent, decompression rates near the vent become sufficiently high to oversaturate inter-bubble melt enough to trigger a second phase of nucleation. This process creates a bi-modal bubble size distribution: pre-eruptive (50-100 μm) and syn-eruptive (10-50 μm). A scanning electron microscope (SEM) was used to examine bubble imprints preserved in volcanic ash particles and determine an explosivity threshold, represented by the volcanic explosivity index (VEI), below which decompression rates are too slow for a second nucleation event to occur. This threshold is manifested in ash particles as a lack of syn-eruptive bubbles and was found to be between VEI 3 and 4. Furthermore, examination of ash from six eruptions (Redoubt, Spurr, Augustine, Okmok, Novarupta-Katmai, and St. Helens) indicates that eruptions with a higher VEI (e.g., Novarupta-Katmai, VEI 6) have a higher percent of observed particles displaying syn-eruptive bubbles than lower VEI eruptions (e.g., Redoubt, VEI 3). This may reflect a decompression rate gradient horizontally across the conduit during magmatic ascent. For eruptions with higher bulk decompression rates, a larger cross-sectional area of magma within the conduit was able to overcome the slowing force of shear created by this gradient, and decompress rapidly enough to nucleate syn-eruptive bubbles.

Furthermore, Micro Raman data show the presence of water in ash from some eruptions (Spurr, Okmok), indicating that magmatic water is still present in some systems upon eruption, and also alluding to complex diffusion and nucleation

mechanics. This study advances understanding of the relationship between eruptive products and eruption energetics; this provides a tool to better constrain eruption energetics of ancient eruptions, and thus to better characterize volcanic activity in the past in order to project it to eruption hazards in the future.

1. Introduction

Violent volcanic eruptions pose some of the greatest geologic threats to society through impacts on agriculture, infrastructure, and human health, but are often too violent to directly observe associated eruption energetics and vent velocities via real-time instrumentation, making prevention of these threats difficult. As a result, it is necessary to use proxies by which eruption energetics can be determined. This study develops one such proxy by characterizing the relation between eruption mechanisms, which occur within the conduit to promote fragmentation and therefore produce ash, and the morphology of ash particles, which are ejected into the atmosphere and pose economic and health hazards. This study also seeks to introduce the use of water preserved in volcanic ash particles as a secondary proxy of eruption energetics. Using associated eruptive products, this study reconstructs relative vent velocities of known past explosive volcanic eruptions, and provides the ability for similar methods to be used to make predictions of volcanic energies for future eruptions. This tool is particularly useful for the determination of eruption explosivity characteristics of pre-historic eruptions for which little information is available. This provides volcanologists with a new tool by which to measure eruption energetics and associated fragmentation processes. It represents a significant advancement in our understanding about the relationship between eruption processes and eruptive products, and is an important step forward in terms of hazard prediction and mitigation.

2. Background

2.1 Ash Morphology:

Bubbles preserved in volcanic ash particles would seem to be records of intra-conduit processes. Previous studies have done extensive work on the nucleation and growth of bubbles in magma as it ascends through a conduit (e.g., Genareau et al., 2012; Gonnermann, 2015; Gonnermann & Houghton, 2012; Koyaguchi, 2005; Larsen, 2016; Massol, 2004; Massol & Koyaguchi, 2005; Pistone et al., 2016; Proussevitch & Sahagian, 1996, 1998; Toramaru, 2014). Bubbles nucleate in magma during ascent when pressure decreases sufficiently below the saturation pressure to overcome surface tension pressure. The details of this process are poorly understood, yet nucleation does occur as bubbles exist in magmas. Nucleation typically occurs at a depth of 8-5km due to decompressive ascent (Koyaguchi, 2005). The growth of these bubbles, termed “pre-eruptive” bubbles, drives the ascent of overlying magma and the bubbles it contains. These bubbles grow further in a positive feedback due to their own accelerating decompression and the diffusion of volatiles (typically water) out of the melt and into the bubbles due to reduction in solubility during decompression (Genareau et al., 2012; Proussevitch & Sahagian, 1996, 1998). During this process, water diffuses from bubble walls towards existing bubbles, serving to decrease water concentrations in the melt (Massol & Koyaguchi, 2005). This continuum of growing bubbles results in ascent at the vent that can be so rapid that the melt again becomes supersaturated (Massol, 2004). In this situation, water cannot diffuse into the growing

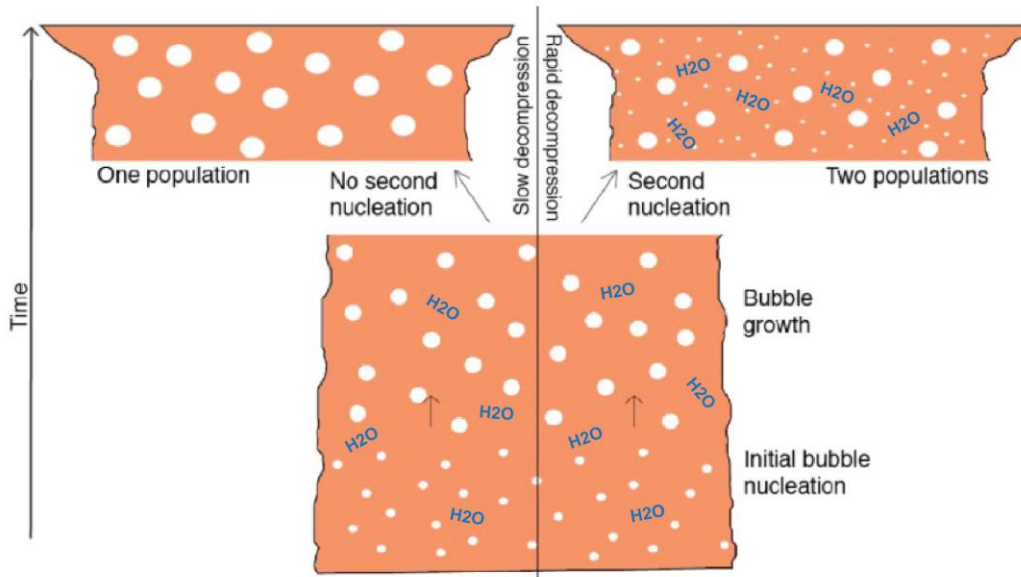


Figure 1: Conceptual model of conduit processes. The initial stages involve bubble nucleation at depth and volatile diffusion to pre-existing bubbles. With relatively slow decompression (left side), volatiles diffuse into these bubbles throughout the history of magma ascent and decompression, and only one size population of bubbles is observed in erupted products. With relatively rapid decompression (right side), volatiles do not have sufficient time to diffuse into pre-existing bubbles, so magma becomes sufficiently oversaturated to nucleate a second phase of bubbles, which are very small and numerous. These are termed syn-eruptive bubbles. With extreme eruption rates, volatiles may remain in the melt upon fragmentation and quenching.

bubbles fast enough to prevent oversaturation from exceeding the threshold for nucleation. If this occurs, a second nucleation event takes place, creating a very large number of very small bubbles ($<10\text{-}50\mu\text{m}$), termed “syn-eruptive” bubbles (Toramaru, 2014, Genareau et al., 2012). These bubbles form in regions of inter-bubble melt that are not yet depleted of volatiles by diffusion into bubbles; in these areas, magma still is saturated with volatiles, and becomes oversaturated with further decompression (**Figure 1**; Gonnermann & Houghton, 2012). This oversaturation occurs near the point of magma fragmentation, when the decompression rate often increases more than two orders of magnitude (Massol & Koyaguchi, 2005). At the point of fragmentation,

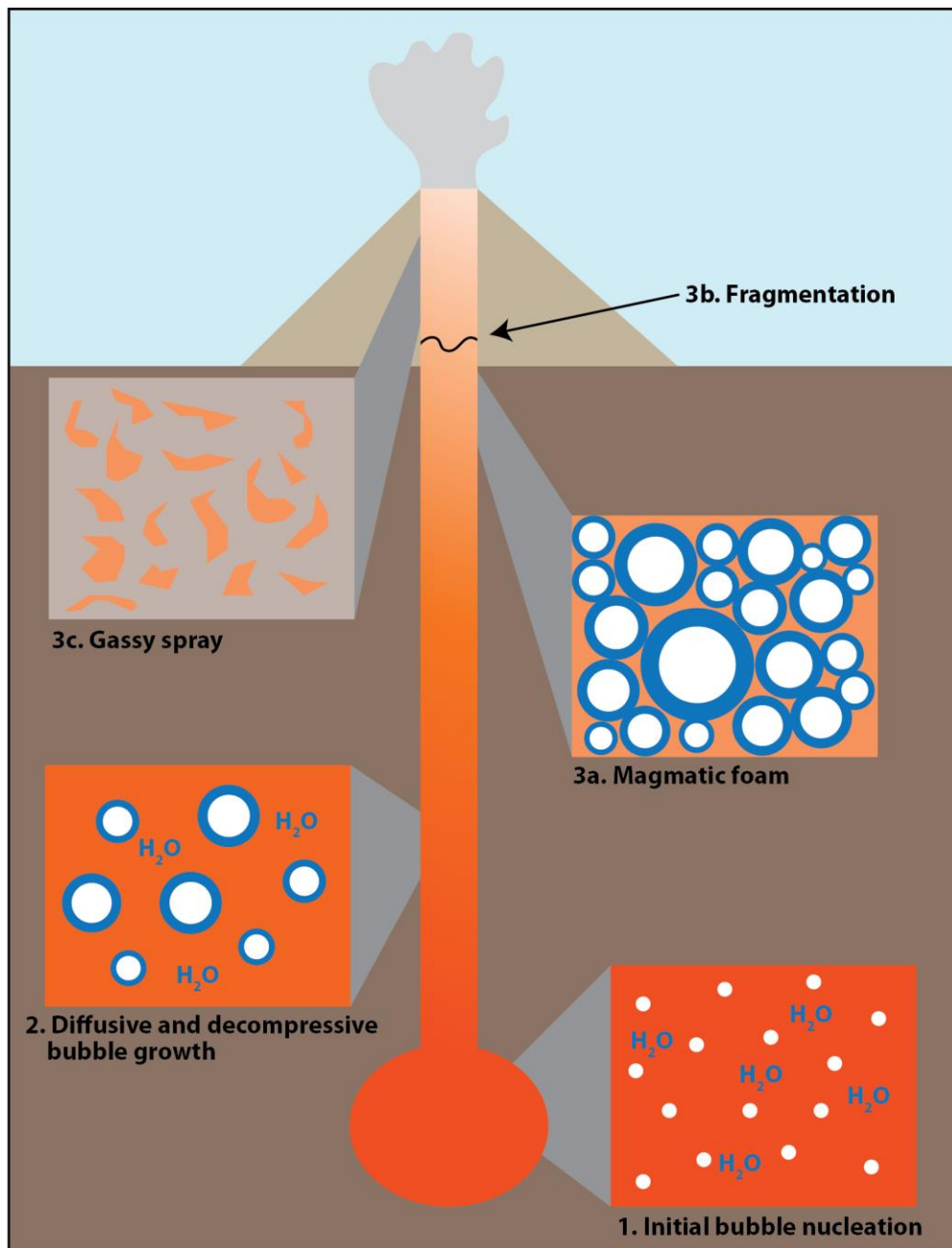


Figure 2: Schematic diagram of magma rising through the conduit and reaching the point of fragmentation. 1. Initial bubble nucleation with volatiles remaining in the melt, 2. Bubbles grow via diffusion of volatiles out of the melt and decompression, 3a. Magmatic foam consisting of large, growing bubbles with thin walls of viscous magma in between them, 3b. Magma fragmentation due to tensile stresses exceeding tensile strength of the magma, 3c. Resulting gassy spray consisting of fragmented bubble walls entrained in a high-energy gas. (Adapted from Sahagian, 1999).

magma within the conduit transitions from a laminar flow composed of a viscous, bubbly liquid (magmatic foam), into a turbulent flow of liquid fragments entrained in gas (gassy spray), due to a high gas volume fraction (**Figure 2**; Massol & Koyaguchi, 2005; Proussevitch & Sahagian, 1993). This happens as a result of gas expansion, and thinning and disruption of bubble walls, with subsequent release of gas from confining bubbles, as tensile stresses overcome magmatic tensile strength and the material undergoes brittle fracture (Gonnermann, 2015; Zhang, 1999). It is estimated that the vast majority of syn-eruptive bubbles from very energetic eruptions nucleate within a time interval of ~0.1 seconds (Gonnermann & Houghton, 2012). This suggests that the second nucleation event is truly an entirely separate occurrence and not part of a continuum of bubble growth such as that for pre-eruptive bubble nucleation. This second nucleation, in turn, greatly increases the energy of the eruption because this new population of bubbles provides buoyancy and further over-pressurization of the ascending magma (Toramaru, 2014). Modeling of nucleation conditions suggests that the peak in nucleation coincides with the peak in bubble and fragmentation overpressures, thus the nucleation of a large portion of bubbles happens very near the time of fragmentation (Gonnermann & Houghton, 2012). This relationship supports the idea that late-stage bubble nucleation and fragmentation create a positive feedback loop (Gonnermann & Houghton, 2012). Examination of pumice clasts containing syn-eruptive bubbles reveals high internal gas pressure in these bubbles, indicating the limited ability of gas to further expand during rapid decompression (Massol &

Koyaguchi, 2005). This indicates that the nucleation process plays a role in overpressurization and thus magma fragmentation, supporting the linked nature of syn-eruptive bubble nucleation and fragmentation (Massol & Koyaguchi, 2005).

Fragmentation induced by overpressure not only occurs because of rapid magma ascent and thus decompression, but can also be applied to systems involving rapid decompression of stationary magma (Gonnermann, 2015). This suggests that the outlined bubble nucleation and fragmentation framework can be applied for a wide range of volcanic eruption types, including those such as Mt. Saint Helens, which involved rapid decompression due to sector collapse (Gonnermann, 2015).

Previous studies have established a relationship between bubbles that get preserved in volcanic ash as vesicles and the energetics associated with an eruption (Toramaru, 2006). The bubble number density (BND) has a strong positive correlation with decompression rates, and thus with eruption column height (Toramaru, 2006). While this study focuses on complex ash particles, similar studies have been conducted on simple ash (Genareau et al., 2012). Complex ash can be defined as showing multiple relict bubble walls (vesicles) that burst during fragmentation, whereas simple ash records only one vesicle on each exterior surface (Genareau et al., 2012; Genareau et al., 2013). These intra-conduit bubble nucleation processes can create a bimodal bubble size distribution in sufficiently explosive eruptions (Genareau et al., 2012). These two nucleation stages and their resulting bubble sizes are described as pre-eruptive (early-stage and relatively large, $>50\mu\text{m}$), and syn-eruptive (late-stage and very small, $<10\text{-}50\mu\text{m}$), to distinguish the timing and processes that create each

population (Genareau et al., 2012). In cases where decompression rates were high enough to allow the second nucleation to occur, there is typically a much larger number of syn-eruptive than pre-eruptive bubbles (Toramaru, 2014). It is estimated that the second nucleation producing numerous small bubbles requires decompression rates that are at least 10 times higher than those required to nucleate pre-eruptive bubbles (Toramaru, 2014). This is because the first generation of bubbles makes it possible for water to readily diffuse into existing bubbles, thus limiting water oversaturation in the melt during subsequent decompression. If decompression rates are not sufficiently high to generate syn-eruptive bubbles in a less energetic eruption, the eruption will proceed with only the growth of pre-existing bubbles because volatiles will have enough time to diffuse into pre-existing bubbles. In this case a second nucleation will not be apparent in ash particles.

2.2 Water Content:

Water preserved in volcanic ash is another indicator of eruption energetics. Magmas contain water in predominantly molecular form (H_2O) but also in hydroxyl form (OH^-) as well. Typically, during bubble nucleation, water diffuses toward existing bubbles (Massol & Koyaguchi, 2005). When decompression rates are high enough for a second bubble nucleation to occur, water may be preserved in inter-bubble melt, after fragmentation at the time of quenching, because of a lack of time to diffuse into bubbles. As a result, water content in ash particles may reflect decompression and quenching rates due to the time-limited ability of diffusion.

Therefore, the water content of ash should increase with eruption energy. Previous studies have successfully measured water content in other volcanic products such as obsidian (Dunbar & Kyle, 1992), pumice (McIntosh et al., 2014), and fluid inclusions in phenocrysts (Hervig et al., 1989), indicating that water in glass can be measured. However, surprisingly, no one has collected such data for volcanic ash.

One study measured water concentration gradients around vesicles in laboratory-created volcanic pumice and found the highest concentration to be at bubble walls, indicating resorption during cooling (McIntosh et al., 2014). This resorption occurs because water solubility in glass increases with decreasing temperature and increasing pressure. In this case, temperature was found to be the dominant control (McIntosh et al., 2014). Experimental conditions used to test resorption were 825-1050°C and 56-100MPa (McIntosh et al., 2014). During quench, molecular water diffuses out of bubbles and back into the melt before the particle cools completely (McIntosh et al., 2014). Other studies have examined the diffusivity of meteoric water into volcanic pyroclasts in a post-depositional setting (Giachetti & Gonnermann, 2013). If this were the case for the ashes in the present work, it would pose problems, as we seek to determine water content in the magma at the time of eruption and quenching. However, diffusion of meteoric water into ash particles has been found to occur on timescales too short to affect the data obtained in this study. Water diffusivity decreases dramatically as temperature decreases; at 30°C diffusivity is only $\sim 10^{-21}$ m²/s, meaning it would take ~ 30 years for enough water to dissolve into the particle to create a 1µm-deep halo of water resorption on the surfaces of ash

particles (McIntosh et al., 2014). Given the size and very young age of ash particles in question in this study (~200 μm), this water diffusion can be taken as negligible. However, using water as a stand-alone proxy for pre-historic eruption energetics should be done carefully, as ash from very old eruptions may no longer be representative of magmatic water content at the time of fragmentation due to this resorption.

2.3 Volcanic Explosivity Index:

A popular description of the energy of volcanic eruptions is the Volcanic Explosivity Index (VEI). The VEI is essentially analogous to the Richter magnitude scale for describing earthquakes. VEI ranges from 1-8, with 1 being the least explosive and 8 being the most explosive. Each step up on the VEI scale implies a 10x increase in explosivity. However, it is only a loose proxy for decompression rate because it is based on eruption plume height, the volume of eruptive products, and the duration of the eruption. The index was initially intended for use as a measure of the impact of volcanic eruptions on climate, *not* as a fundamental basis on which to judge the explosive power of volcanic eruptions and thus assess related hazards (Newhall & Self, 1982). The VEI was nevertheless a step forward in our understanding of eruption energetics. Most previous studies of explosivity, before the index was developed in 1982, were based solely on volume of erupted products (Newhall & Self, 1982; Tsuya, 1955). This approach is problematic for two reasons: first, it requires complete knowledge of the volume of erupted products. Obviously, for pre-historic eruptions,

this is impractical due to the prevalence of erosion and mixing, as well as deposition in the ocean or other bodies of water. Thus it is impractical to use estimates of the volume of ejecta products from pre-historic eruptions as the sole basis upon which the eruption's energetics are described (Newhall & Self, 1982). Secondly, relying solely on estimates of the volume of eruption products would over-emphasize effusive eruptions, which can be quite voluminous. Therefore, the *explosivity* of an eruption would not truly be described, but rather something more like the eruptive magnitude, which is determined from the volume of ejecta (Newhall & Self, 1982). Therefore, by considering other parameters such as column height, qualitative descriptors such as eruption type, and duration, the VEI scale accounts for facets of an eruption that are more representative of *explosivity*.

While the VEI scale was a step forward in understanding relative eruptive energies, it still fails in its over-emphasis on the volume of ejecta. Newhall and Self (1982) identify this parameter as the most reliable in evaluating volcanic explosivity, with column height being the second most reliable (Newhall & Self, 1982). Others suggested that column height is likely more reliable, as it is directly related to decompression rate, which truly is a quantitative measure of an eruption's explosivity (Toramaru, 2006). This bears on the present study for two reasons: First, the factors that the VEI scale relies upon need to be delicately parsed out on an eruption-by-eruption basis if VEI is to truly be the standard of explosivity to which we correlate our results. For example, if one eruption is classified at a certain value because of its tall eruption plume, but another is classified as such because of its long duration of

eruption, then the eruption with the higher plume should be considered more energetic (Toramaru, 2006). Therefore, plume height should dominate VEI because it provides a reliable measure for eruption energetics, and can provide a direct link to decompression rates and exit velocities at the vent (Toramaru, 2006). This will be further explained in the discussion section, as we consider some of the complications arising from different parameters used to calculate VEI. Also, by using plume height as a measure of explosivity, we can still see the need for another proxy such as the one developed in this study: plume height, like the other factors that contribute to VEI, can be directly observed only in real time during eruption. Therefore, the need exists to determine eruption energetics from eruptions that have not been witnessed directly, in order to determine the relative explosivities of ancient eruptions and provide insight regarding how explosive those volcanoes might be if they again erupt. This study seeks to directly compare physical and chemical properties of ash to eruption energetics, namely decompression rates and their expression as vent velocity. I seek to use characteristics of eruption mechanics that are capable of being directly preserved in ash particles, and held there as a record of historic and pre-historic eruptions, as a means of describing explosivity. The VEI is simply the closest commonly used scale available at the moment for quantifying eruption energetics.

Regarding the use of the VEI scale, there is an interesting conundrum involving VEI 2 eruptions. Historic and prehistoric eruptions known to have been explosive, but for which no other information is known or possible to collect, are automatically assigned a VEI of 2 (Newhall & Self, 1982). This clearly is problematic

because it has the potential to grossly underestimate the explosive potential of volcanic systems that could be highly explosive and pose an extreme risk, yet for which not much is known. This lack of knowledge could be due to remote location, the eruption being prehistoric, or the lack of well-preserved ash and other eruptive products from which to estimate the volume of ejecta. This study at hand did not directly address this point, as no VEI 2 eruptions were examined, under the assumption that they would be too low-energy to nucleate syn-eruptive bubbles. However, this assumption may be invalid in some cases due to the aforementioned information about VEI 2 eruptions. Further studies may want to examine ash from such eruptions to determine a relative explosivity as derived from bubble size distributions, and ultimately better characterize those supposed VEI 2 eruptions about which little is known.

3. Scope and Implications

3.1 Scientific Scope:

This study is a step towards bridging the knowledge gap between eruption mechanisms and how these mechanisms are manifested in eruptive products (**Figure 3**). Ash morphology is dominated by bubble imprints left on particles upon fragmentation. Bubbles drive the fragmentation processes that produce fine ash during a volcanic eruption. Therefore, the use of evidence preserved in eruptive products to establish a systematic relationship between ash morphology and the vent velocity

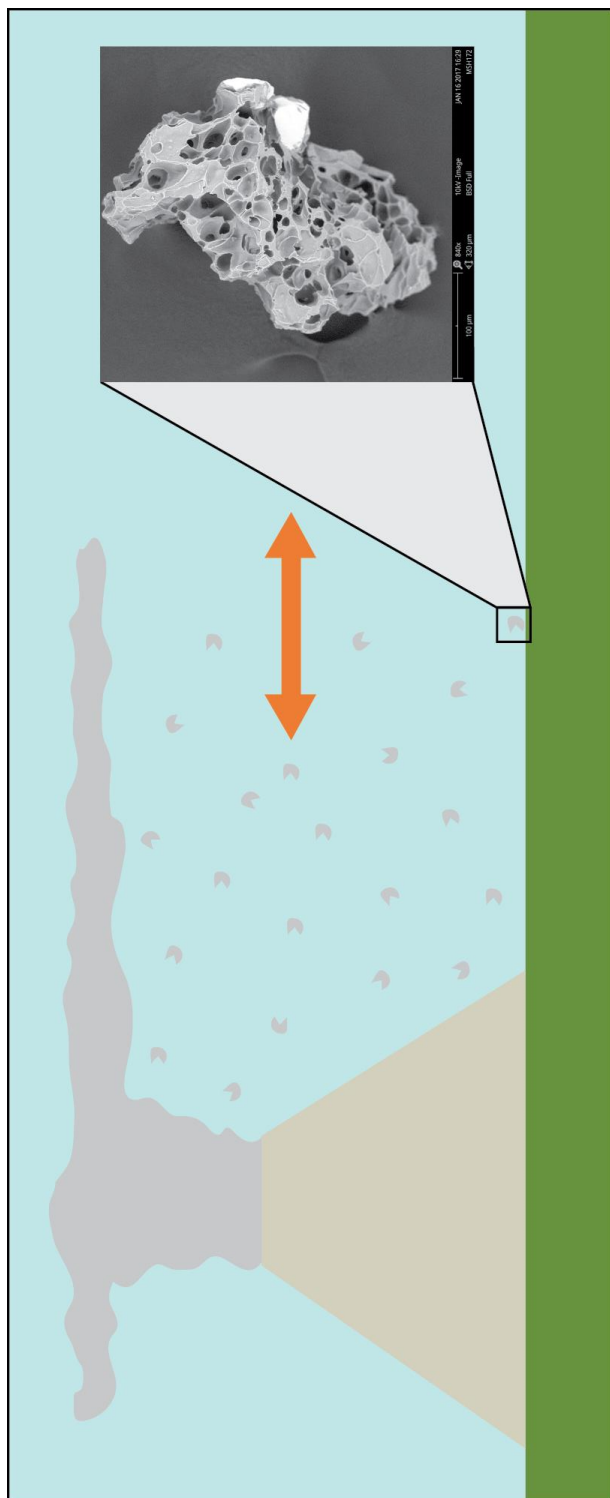


Figure 3: Schematic diagram illustrating the scope of this study. I seek to establish the relationship between ash morphology and eruption energetics. This could allow for ash collected from an eruption to be analyzed and used to better characterize the explosivity of the eruption from which it came.

(decompression rate) contributing to the energy of an eruption, can provide new insight regarding conduit processes during the eruption. Ash morphological data from six volcanic eruptions (Redoubt, Spurr, Okmok, Augustine, Novarupta-Katmai, and Mt. Saint Helens) are a starting point for establishing this connection. Even in these six eruptions, a systematic change in morphology can be observed from lower energy to higher energy eruptions. This dataset can be augmented in the future, with additional eruptions, to create a holistic and comprehensive resource of past eruption energetics useful for assessing future eruption hazards. This can potentially provide the basis for improving volcanic ash transport and deposition models, as these models are based on both eruption energetics and ash morphology. It is important to note that this study is not meant to be a comprehensive analysis of ash morphologies as they relate to eruption energetics; rather, this is an initial conceptual analysis to explore how eruption dynamics can be determined from ash morphology and chemistry.

This study also has the potential to present to the volcanological community a basis upon which to better estimate volcanic explosivities, and may serve as an improvement upon the currently widely used and accepted Volcanic Explosivity Index. This study does not seek to replace the VEI scale, but rather supplement it using physical characteristics in ash as a confirmation of the ability of VEI parameters to describe volcanic explosivities, as well as provide information regarding prehistoric and remote eruptions about which little is known. This point will be discussed in the next section involving societal impacts of the work, as improvement of our understanding of eruption mechanisms and supplementing the toolset by which we

analyze eruption energetics are important not only in a volcanological or even geological sense, but also in a more widespread societal health and impact sense.

3.2 Implications:

The physical mechanisms behind ash production during violent eruptions is an area of volcanology that is poorly quantified, yet one with high-stake societal implications. Improving understanding of how observed eruption processes produce ash can lead to better understanding of particle behavior in the atmosphere, such as ash trajectory, distance traveled, and lifetime in the lower stratosphere and thus air travel safety. The fate of ash depends largely on eruption energetics as well as particle morphology; therefore, understanding the link between these two factors has the potential to greatly improve upon the current understanding of ash behavior in the atmosphere and thus has important societal implications.

Volcanic eruptions are devastating and often unpredictable, and have had large economic and political impacts dating to ancient times (Prata & Tupper, 2009). In the modern, post-industrial era, some of the largest threats that ash poses involve aviation. When aircraft in the stratosphere encounter ash, the ash has the potential to abrade the exterior of the aircraft and enter the engines. Heat from modern, high efficiency engines can cause re-melting of ash, allowing it to coat the interior parts of the engine and lead to a complete loss of thrust (Casadavall, 1994; Hufford et al., 2000). With aviation being so crucial to global travel and transport of goods, this poses serious economic and safety hazards. For example, the 2010 eruption of Eyjafjallajökull in

Iceland halted air travel for weeks because fine ash was suspended in the atmosphere far longer than expected. This disrupted over 100,000 flights in 23 countries, causing the loss of billions of dollars by the aviation industry and thus negative impacts of the global economy. For this reason, Eyjafjallajökull is known as the most disruptive event in aviation history. Volcanic ash can also have direct effects on human economies by damaging infrastructure, particularly vehicles, electric lines, storm drainage systems, and wastewater treatment plants (Wilson et al., 2011). Ash can abrade car engines and clog filters. Very fine ash is extremely effective at coating electrical lines and causing flashover, which is an unintended electrical discharge, and can cause widespread outages. It also easily washes into storm drains, where it can cause widespread clogging leading to extensive flooding. Lastly, it can cause damage to wastewater treatment plants requiring millions of dollars to remediate (Wilson et al., 2011).

The risks of volcanic ash extend well beyond economic. After the 1989 eruption of Mt. Redoubt in Alaska, suspended ash caused one flight to stall in mid-air, with the pilots only able to restart the engines at the last minute before crashing, a consequence that would have been deadly. Ash also poses a risk to human and animal health via direct inhalation of particles or contamination of water supplies with heavy metals leached from ash particles (Horwell et al., 2006; Andronico & Del Carlo, 2016; Graham et al., 1985; Johnston et al., 2004; Stewart et al., 2009). For example, 2% of the ash from the 1980 eruption of Mt. Saint Helens was within the respirable size range ($<3.5 \mu\text{m}$), posing serious and widespread health risks, especially in the densely-

populated Pacific Northwest. Improving understanding of details such as volcanic ash vesiculation processes can lead to a better understanding of particle behavior, and could help decrease the economic and health hazards from future eruptions.

Energetic volcanic eruptions also have potential to inject ash and gasses into the stratosphere, which can have large climatic implications due to long residence times related to the dryness of the stratosphere. Fine ash and clouds of sulfate aerosols can cause cooling at Earth's surface and warming in the stratosphere, disrupting global advection currents (Robock, 2000). Climatic responses to volcanic products represent large-scale perturbations on very short timescales and can have serious effects on the global climate system (Robock 2000). Impacts of volcanism on global climate trends have been extensively studied (Baldini et al., 2015; Santer et al., 2014; Mann, 2007; Robock, 2000). Historically, large eruptions such as Huaynaputina (1600), Laki, (1783), Tambora (1815), and Krakatoa (1883) have produced unseasonably cold regional and global weather, leading to crop failure, famine, and political unrest. More recently, the 1991 eruption of Pinatubo caused widespread cooling in the lower troposphere (Santer et al., 2014). This is an important consideration in modern day climate models describing anthropogenic climate change (Santer et al., 2014). Eruptions examined in this study have also had widespread climatic effects: fine ash and gas injection into the atmosphere from Novarupta-Katmai caused as much as 1°C cooling throughout the Northern Hemisphere (Hildreth & Fierstein, 2012). Better characterizing volcanic explosivities can allow for improved understanding of the potential climatic effects posed by injection of volcanic products into the stratosphere.

The motivation for this study is to eliminate the need to observe volcanic eruptions directly, as is necessary in order to obtain the information necessary to determine a VEI based on volume of erupted product, eruption plume height, and eruption duration. This would allow understanding of the explosivity and thus threat of volcanic systems that may still be active and pose a risk to human health and safety, but for which these measurable data are not available. Current means of estimating the explosivity of historic and pre-historic eruptions may significantly underestimate their VEI based on insufficient information (Newhall & Self, 1982). This certainly could underestimate a significant number of eruptions about which little is known but which may be part of regional volcanic systems posing tangible threats to modern societies.

In order to better constrain pre-historic eruption energies, studies have traditionally used ash thickness and distribution as a means of understanding ancient and remote volcanic eruption energies. More explosive eruptions should disperse ash farther and create thicker ash units at greater distances. However, ashfall thicknesses vary greatly, often due to differences in wind and other weather conditions. Additionally, ash deposits from pre-historic eruptions could have been significantly eroded or otherwise disturbed prior to modern examination, or may have been deposited in the ocean (Newhall & Self, 1982). Newhall and Self describe the task of quantifying relative explosivities of pre-historic eruptions for which little is known as “impossible” (Newhall & Self, 1982). They then present a scale that is developed using all available (witnessed) data (Newhall & Self, 1982). This scale is completely dependent upon the availability of data, assigning VEI’s regardless of comprehensive

and consistent data for every eruption. Variability in available data would certainly lead to variability in the accuracy of assessments made from that data.

To combat this, we present here a new dataset that does not depend on direct observation of eruptions, and that can be consistently collected from all ash-producing eruptions. This approach is truly novel and could have large implications for understanding volcanic explosivity bearing on human health and safety. This method of determining explosivity via erupted products is necessary in order to improve our understanding of eruption explosivities from previous eruptions, and allow for better preparation for potential eruptions, in order to minimize loss of life, health hazards, as well as economic and infrastructure damages.

4. Goals and Hypotheses

4.1 Goals:

The overall goal of this study is to better characterize the energy of an eruption using morphological and chemical data preserved in volcanic ash particles. I sought to use these data to develop new proxies that can supplement accepted measurements of volcanic explosivity, such as the VEI scale. Ideally, for eruptions about which very little is known, these proxies could be applied as stand-alone indicators of explosivities. This study contributes to a better understanding of the connection between eruptive mechanisms and erupted products, as well as an improvement upon current volcanic hazard and prediction models, in the hopes of decreasing the risk to

human health, safety, and economics that presently looms in areas with active or recently-active volcanism.

4.2 Hypotheses:

To achieve this goal, outcomes were broken into four testable hypotheses. These were tested using ash samples from eruptions with known energetics, in order to determine the validity or falsity of such hypotheses. The hypotheses are as follows (in order of increasing complexity and decreasing priority):

Hypothesis #1: There exists a threshold of VEI, loosely representing decompression rate, below which the second nucleation and thus production of syn-eruptive bubbles will not occur. This threshold exists because bulk decompression rates are slow enough to allow time for the vast majority of volatiles in the melt to diffuse into pre-existing bubbles, rather than supersaturating and nucleating new bubbles, as would occur with very rapid decompression rates. This hypothesis was tested using scanning electron microscope (SEM) imaging, observation, and analysis of individual ash particles.

Hypothesis #2: Highly energetic eruptions have a higher fraction of particles that display both pre and syn-eruptive bubbles than lower energy eruptions (**Figure 4**). This is because syn-eruptive bubbles form as a result of extremely rapid decompression rates, limiting the time scale available for volatiles in the melt to

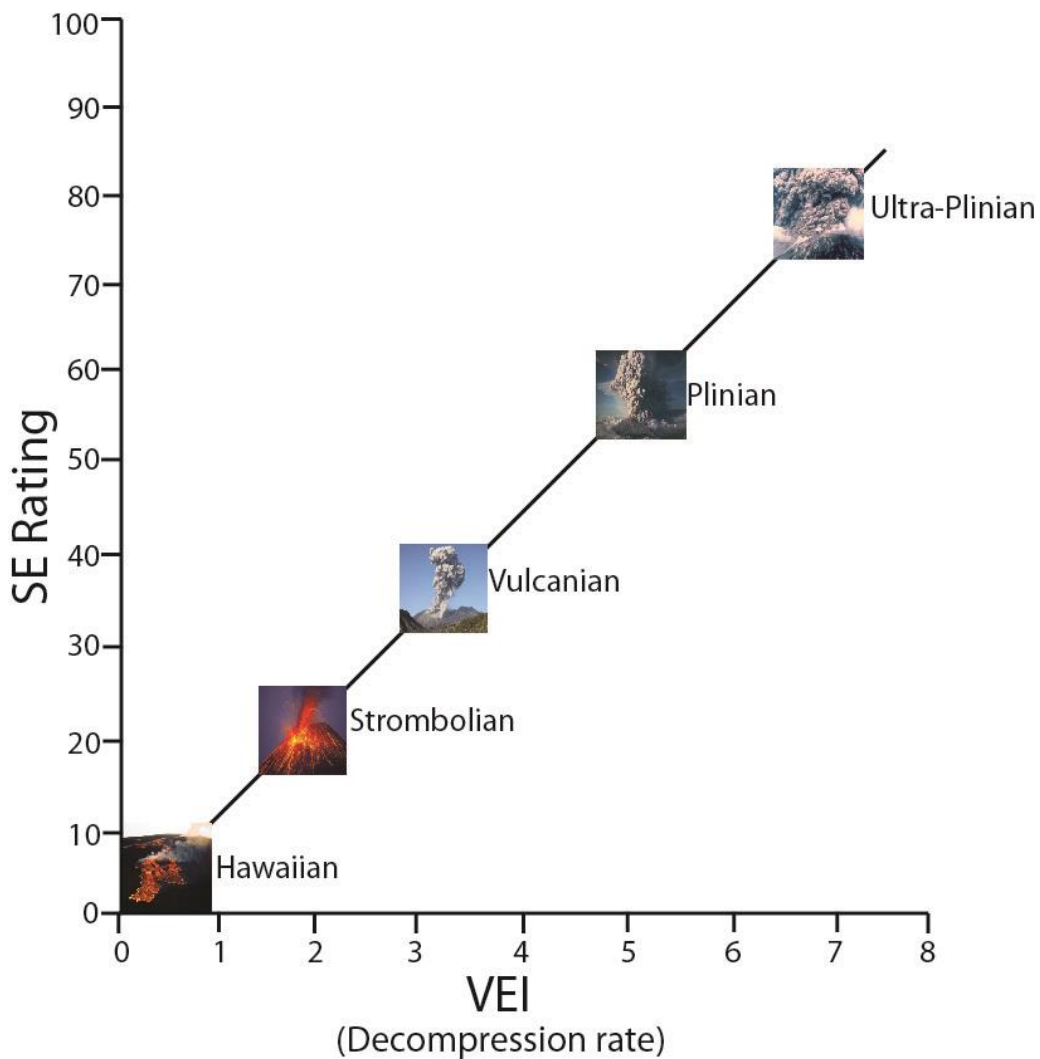


Figure 4: Predicted relationship between decompression rate (represented by VEI) and SE Rating (the percent of examined particles that display syn-eruptive bubbles). The SE rating is expected to increase with increasing decompression rate, and thus increasing explosivity of the eruptive style.

diffuse through the magma and enter pre-eruptive bubbles before reaching critical oversaturation for nucleation. This is tested using scanning electron microscope (SEM) imaging, observation, and analysis of individual ash particles.

Hypothesis #3: Higher eruption energies have higher bulk water content because water does not have time to diffuse into pre-existing bubbles and is quenched in the melt upon fragmentation. This is tested using Micro-Raman Spectroscopy on individual ash particles.

Hypothesis #4: A gradient of molecular water content exists that is highest at bubble walls and decreases into the particle interior due post-fragmentation, pre-quench resorption (McIntosh et al., 2014). This is tested using Micro-Raman Spectroscopy on transects moving away from bubble walls in individual ash particles.

5. Geologic Setting

Details of each eruption for which ash was obtained can be found in **Table 1**. Ash from each eruption was taken from proximal locations. All of the eruptions considered in this study occurred in subduction zone settings. The Aleutian Volcanoes (Redoubt, Spurr, Okmok, Augustine, and Novarupta-Katmai) are the result of the subduction of the Pacific plate beneath the North American plate. Mt. Saint Helens and the other Cascadia Volcanoes are the result of the subduction of the Juan de Fuca plate beneath the North American plate. Mt. Saint Helens (Washington), and Mt. Spurr, Mt. Redoubt, Augustine Volcano, Okmok Volcano, and Novarupta-Katmai (Alaska) all erupted explosively in relatively recent history (**Table 1**), causing damage

Table 1: Summary of eruptive characteristics of eruptions examined in this study.

	Eruption Year	VEI	Plume Height (km)	Volume Erupted (tephra-fall) (m³ DRE)	Composition	Other Info	Reference
Redoubt	2009	3	4.6-18.9	2.06 x 10 ⁷ total	Andesite with intermediate Si content	20 explosions lasting between 1 and 31 minutes	Wallace et al., 2013
Okmok	2008	4	4-11	2.6 x 10 ⁸ total	Rhyodacite to andesite	Abundant tremors and ash plumes occurred episodically for ~1 month	Global Volcanism Program, 2008 and Larsen et al., 2013
Spurr	1992	4	14-15	1.2, 1.4, 1.5 x 10 ⁷ per eruption (41 x 10 ⁶ total)	Juvenile andesite	3 separate eruptions lasting 3.5-4.0 hours each	Eichelberger et al., 1995 and Neal et al., 1995
Augustine	2006	4	3.8-16	8.5 x 10 ⁶ total during explosive phases	Low to high silica andesite	4 eruptive phases, with the explosive phase consisting of 13 Vulcanian explosions	Wallace et al., 2010
Mt. Saint Helens	1980	5	14-24	2.0 - 2.5 x 10 ⁸ total	Dacite to andesite	9 hour Plinian eruption subdivided into 6 phases based on eruption style	Carey et al., 1990, Criswell, 1987, and Sarna-Wojcicki et al. 1981
Novarupta-Katmai	1912	6	17-26	6.5 x 10 ⁹ total	~55% rhyolite, ~35% dacite, ~10% andesite	~60 hour duration consisting of 3 discrete explosive episodes	Fierstein & Hildreth, 1992 and Hildreth and Fierstein, 2012

to health and the economy via dispersal of fine ash particles. These vulcanian to plinian eruptions had VEI's ranging from 3 (Redoubt) to 6 (Novarupta-Katmai). For each recent eruption of these volcanoes, studies have been conducted on the size, distribution, and characteristics of ash (Fierstein and Hildreth 1992; Fruchter et al. 1980; Neal et al. 1995; Wallace et al. 2010; 2013).

6. Methods

6.1 Ash Morphology:

Ash samples were obtained from Kim Genareau at the University of Alabama. All ash samples had been collected within a few hundred km of the vent (thus proximal). A desktop Phenom XL scanning electron microscope (SEM) at Lehigh University was used to obtain detailed images of ash particles. Ash particles were mounted on a small metal stub using carbon tape. Because particles are so small, it would be difficult to manually place a certain number of particles on the stub with any accuracy. Therefore, particles were simply sprinkled from vials onto the stubs, with effort being made to get an even distribution of particles throughout the surface area of the stub. Particles were analyzed using a 10-15kV beam and with the instrument in "Image" or "Point" mode, depending on the beam strength. General scanning across stubs was done in live image quality, while zoomed-in analyses and images were captured in the best image quality mode. The whole imaging process was done in a low vacuum setting. In order to obtain the highest accuracy in terms of imaging all

available particles, a wide view scan was done linearly across the stub in several rows, to image the entire surface. Once a particle was spotted, the instrument was zoomed and focused to get an appropriate scope and clarity on the particle. An image of each viewed particle was saved for reference. During analysis, the size distribution of bubbles on the surfaces of individual ash particles was analyzed. I also recorded data regarding bubble spacing, particle size, and other qualitative and quantitative observations about each particle. It was initially questioned whether the vesicles visible on the surface of ash particles would be truly representative of the size distribution of vesicles throughout the entire particle. Other studies have found via stereological analyses that it is much more likely that quasi-spherical objects (i.e. pre-eruptive bubbles) would be cut along “tropical latitudes” than cut randomly along small circles (Sahagian & Proussevitch, 1998). As such, given a bimodal bubble size distribution, the chances of large, pre-eruptive bubbles being cut along a small circle so that they would appear to be small, syn-eruptive bubbles is so small, that the number of pre-eruptive bubbles that would be cut in such a way can be viewed as negligible, and should not influence the results of this study. Therefore, bubble imprints that are observable on the surface of ash particles via SEM are representative of the true populations of large and small bubbles. The number of particles that clearly displayed both pre-eruptive and syn-eruptive bubbles were counted and recorded. Data were then processed to determine the percentage of total particles per eruption that display pre and syn-eruptive bubbles. In this thesis, I refer to this percentage as the “Syn-Eruptive Bubble Rating” or the “SE Rating.”

6.1.2: SE Rating

The SE rating was used as a measure of what portion of ash particles display both pre and syn-eruptive bubbles. It was correlated with known VEI for each eruption to determine a systematic relationship between syn-eruptive bubble nucleation and the explosivity of an eruption. The SE rating was also used to determine the threshold below which the second nucleation cannot occur, as denoted by zero or very few syn-eruptive bubbles total in a given eruption, and a very low SE rating.

Because our samples represent the full thickness of an ash deposit, they do not record any stratigraphic information, and as such do not allow for detection of temporal variation in eruption characteristics. Therefore, the SE rating derived from these samples is a temporal integration across the entire eruption duration. This builds into the SE rating an overall eruption energy factor, as what matters for overall eruption hazards is the amount of ash that is ejected into the stratosphere for dry transport. This is a product of vent velocity (decompression rate) integrated over the course of an eruptive episode because the eruption column depends on time-integrated flux in order to sustain itself. Therefore, the SE rating is representative of the decompression rates producing syn-eruptive bubbles and does not vary with time.

6.2 Water Content:

I use the term “water content” loosely here, as it was dubious from the start whether it would be possible to detect water in ash using Micro Raman Spectroscopy,

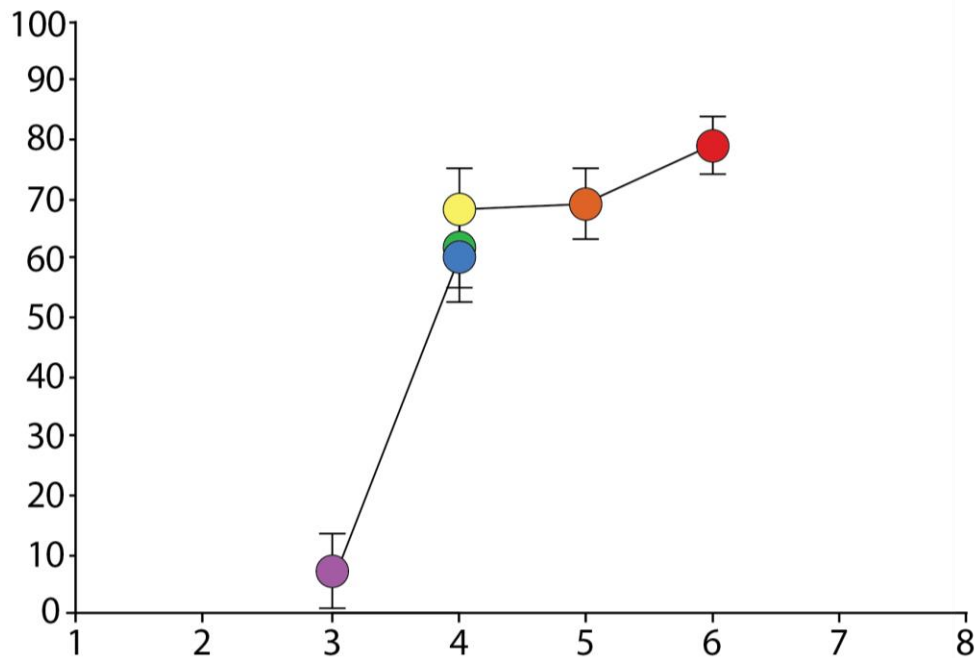
much less whether it would be possible to then derive water contents from those data. In order to explain the Micro Raman methods that I used, it is first necessary to establish some background information about Micro Raman itself. Micro Raman Spectroscopy (and Raman Spectroscopy) is based on the Raman effect, which describes the way that light can scatter inelastically as the result of being focused into a piece of matter. When photons are focused into a piece of matter, they tend to scatter elastically, also known as Raleigh scattering; the scattered photons have the same wavelength as the incoming source. However, about 1 in a million of those photons will scatter inelastically, also known as Raman scattering; in this situation, scattered photons have a wavelength that is slightly shifted from that of the incoming source. This most commonly is manifested as a Stokes shift, in which the scattered photon has a lower wavelength than the incident photons. The magnitude of this shift depends on which type of bond, and thus which molecule the incident photons interact with to cause this inelastic scattering. Not all molecules will cause inelastic scattering, but many will, and those that do will induce characteristic shifts in wavelength. Therefore, the presence or absence of a Raman scatter-inducing molecule can be detected using this method. Micro Raman specifically uses a Raman Microspectrometer, which is simply a Raman Spectrometer in tandem with an optical microscope, to allow for very specific analyses of microscopic samples, or a very small portion of a larger sample. This proved useful to this study because it allowed for analyses of individual ash particles (in the order of 100's of μm) similar to the utility of using the SEM to image individual ash particles to detect the presence or absence of syn-eruptive bubbles.

For my analyses, I used a WITec alpha300 RA Micro Raman at the Lehigh University Physics Department. Ash from each eruption, and from the same vials (and thus with the same sample timing and location) as that used for the SEM portion of this study was carefully placed on glass microscope slides. No epoxy was used. The reasoning for the lack of epoxy was twofold: 1. Epoxy can sometimes interfere with the signal from the sample, causing the detection of molecules that may not be present in the actual ash sample, or simply by adding additional noise and complicating the signal from the ash sample, and 2. If enough care is taken between sample preparation and loading onto the microscope, the ash sticks to the slide via simple static electricity. A prepared sample was then loaded onto the microscope with the light focused on a visible particle on the slide. I began with the 10x objective and carefully focused so that the particle, or at least part of the particle, was in focus. Because of the depth sensitivity of the Micro Raman laser, it was important to focus on the flattest horizontal part of the particle, in order to ensure that the laser was focused entirely across the breadth of its footprint. It was also important that we were sure that the spot that we chose to focus on is actually ash and not an inclusion. Once a spot on the particle was in focus on the 10x objective, we gradually increased magnification to 20x and then 50x, with minor refocusing upon each magnification increase. It was important that the optical focus was done properly because the machine used this to know where the laser should be directed. If the microscope was out of focus (too far up or down in the z direction), the laser could have been transmitted to the space above the sample or too deep within the sample. Once the 50x objective was in place

and the microscope was focused on a specific, somewhat flat section and inclusion free point on the particle, the microscope was switched to dark mode, which inhibits viewing of the particle. The laser was then opened and the machine was directed to obtain a single spot spectrum, which would fire the laser at the location that was in focus and record inelastic scattering from this point. For these experiments, a 532 nm (green) laser was used to excite the sample because this frequency most effectively excites the O-H bond of the water we seek to measure. For each spot, I used an integration time of 10 seconds and obtained 20 accumulations, in order to collect enough repeatable data from the spot to produce a reliable spectrum of inelastic scattering. For many samples, this process was done on the surface of the particle (denoted by the optical focusing on this spot). I subsequently moved inside the particle in 3 μ m increments in order to detect any changes in water concentration moving inwards from the particle. The maximum depth we measured was 12 μ m. After this point, produced spectra became too noisy due to scattered protons passing back through the particle during scattering. I repeated this same procedure on several ash particles per eruption in order to obtain a characteristic water concentration and depth profile of water in ash for each eruption.

7. Results

7.1 Ash Morphology:









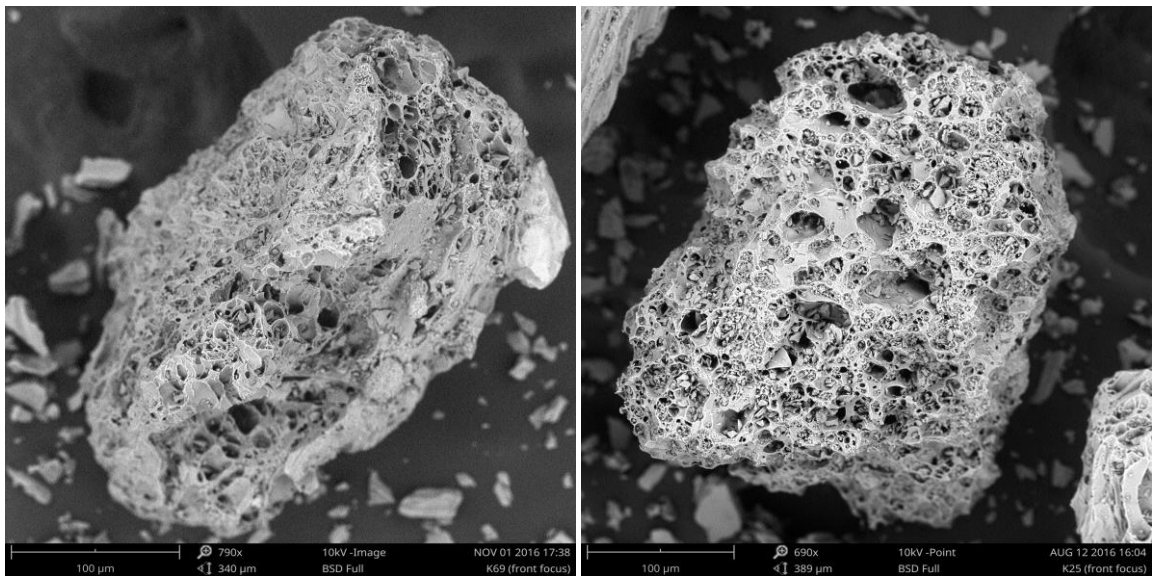
	Name	Symbol	VEI	SE Rating	\pm
	Redoubt	●	3	7	6
	Spurr	●	4	60	8
	Okmok	●	4	61	7
	Augustine	●	4	68	7
	St. Helens	●	5	69	6
	Katmai	●	6	79	5

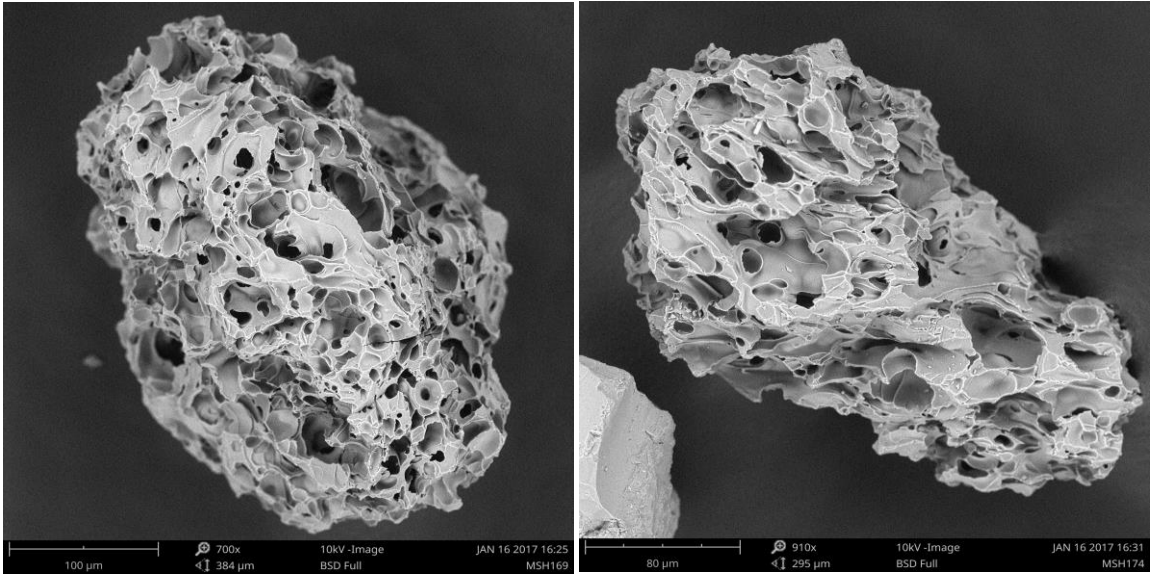
Figure 5: Summary of results from the ash morphology portion of this study. The table is plotted in the chart. Data shows a clear threshold of decompression rates below VEI 4, and gradual scaling of increasing SE rating with decompression rate for eruptions VEI 4-6. Error was calculated using percent of particles for which classification was more difficult. Classification parameters were kept consistent throughout analysis; therefore, likelihood that SE Ratings fall elsewhere besides the plotted points is very low.

A summary of results can be found in **Figure 5** and images of ash particles can be found in **Figures 6a-6f**. As expected, Redoubt (VEI 3) has a very low syn-eruptive rating of 7. Only 6.7% of examined particles from Redoubt clearly contain syn-eruptive bubbles. The SE ratings for other the eruptions scale up as energy increases. Spurr, Okmok, and Augustine (all VEI 4) have SE ratings of 60, 61, and 68, respectively. Mt. Saint Helens (VEI 5) has a SE rating of 69. Lastly, Katmai has a SE rating of 79. Size ranges of measured particles are ~50-900 μ m. Novarupta-Katmai, Saint Helens, and Augustine also display generally more numerous and closely spaced syn-eruptive bubbles than Okmok and Spurr. All ash morphology data can be found in **Appendix 1**.

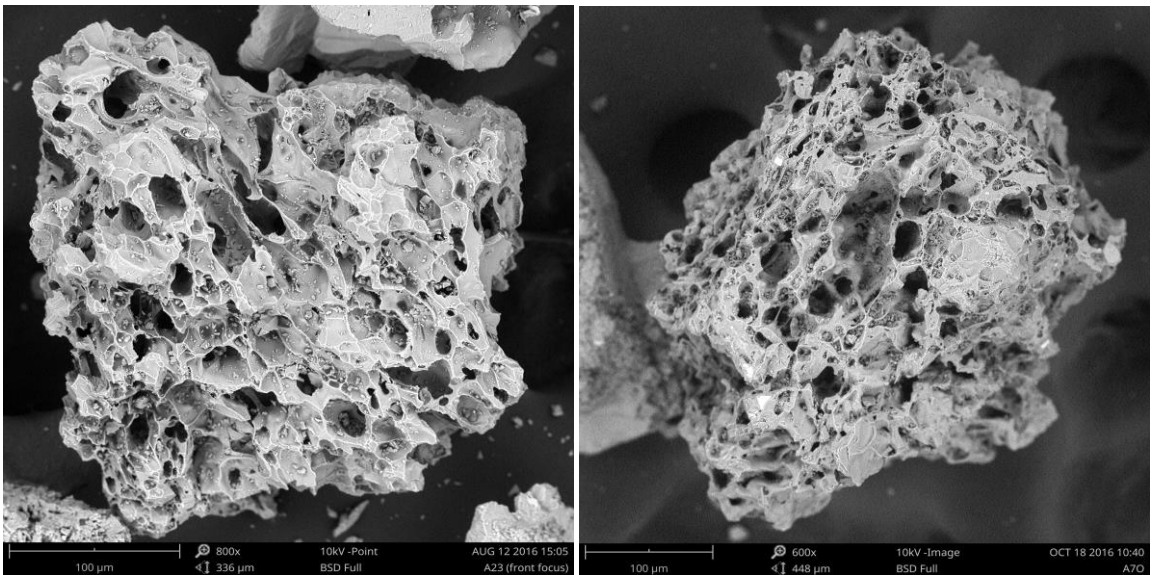
(a)



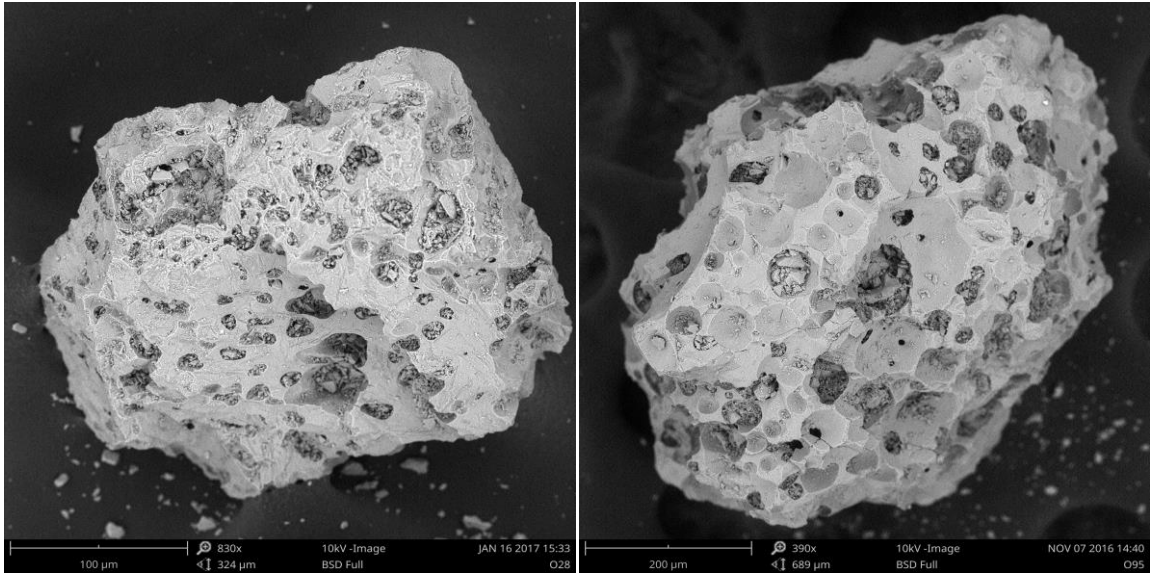
(b)



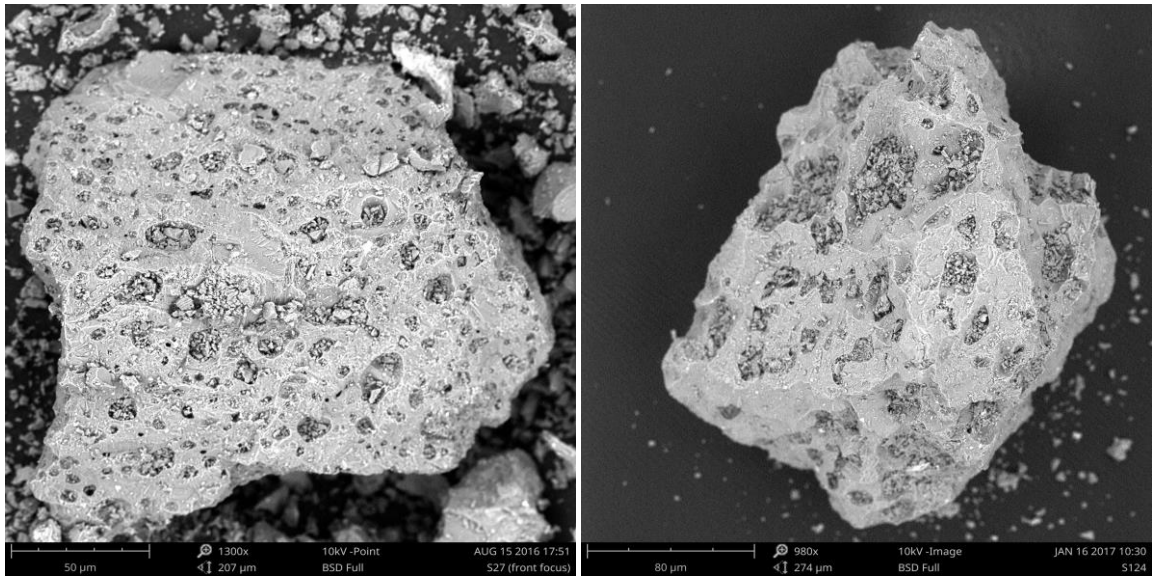
(c)



(d)



(e)



(f)

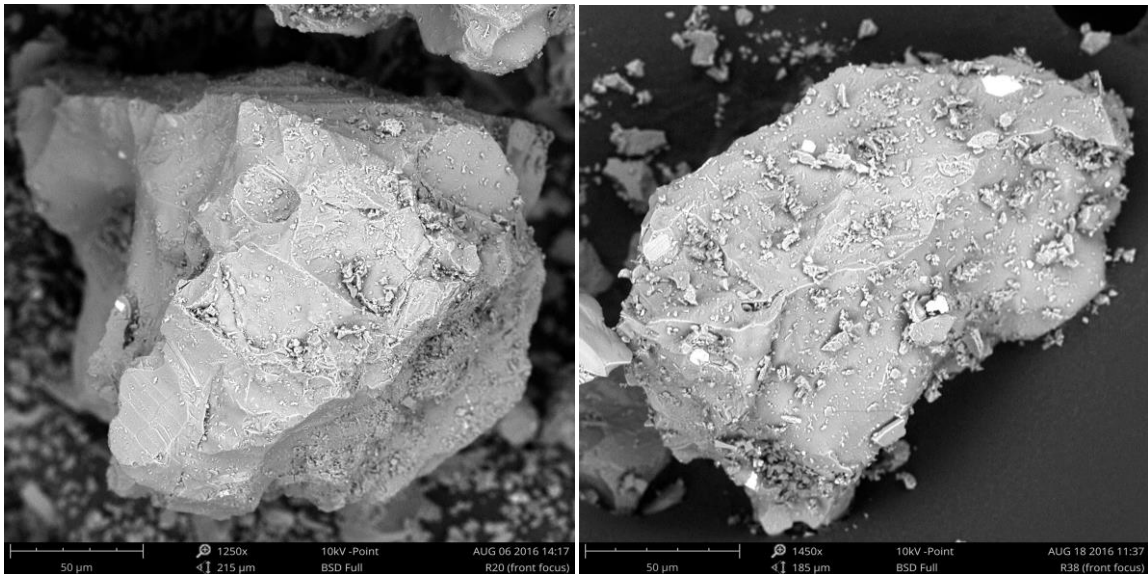


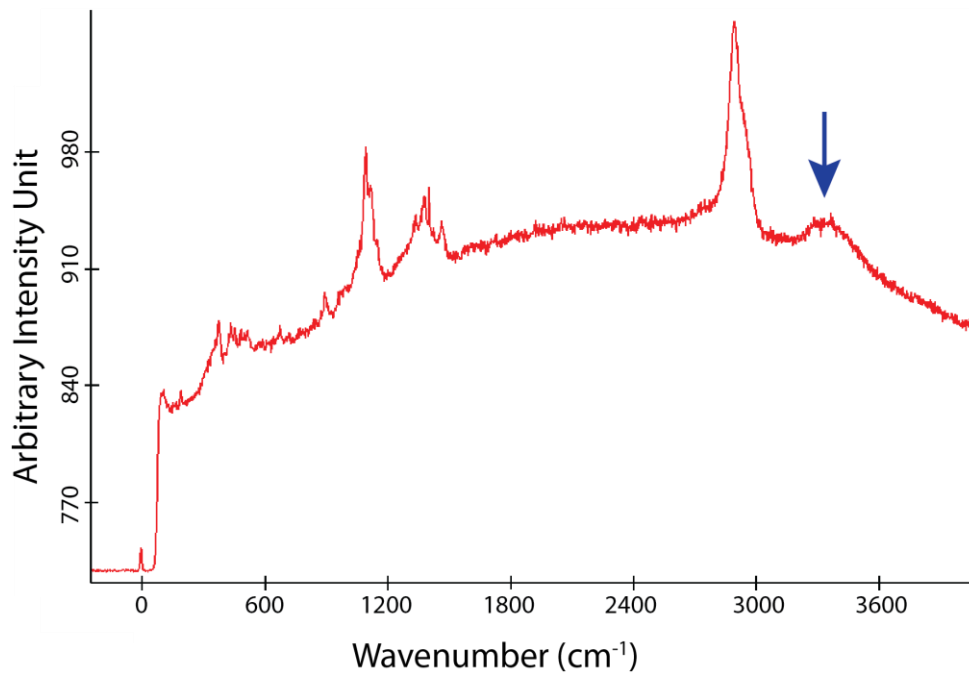
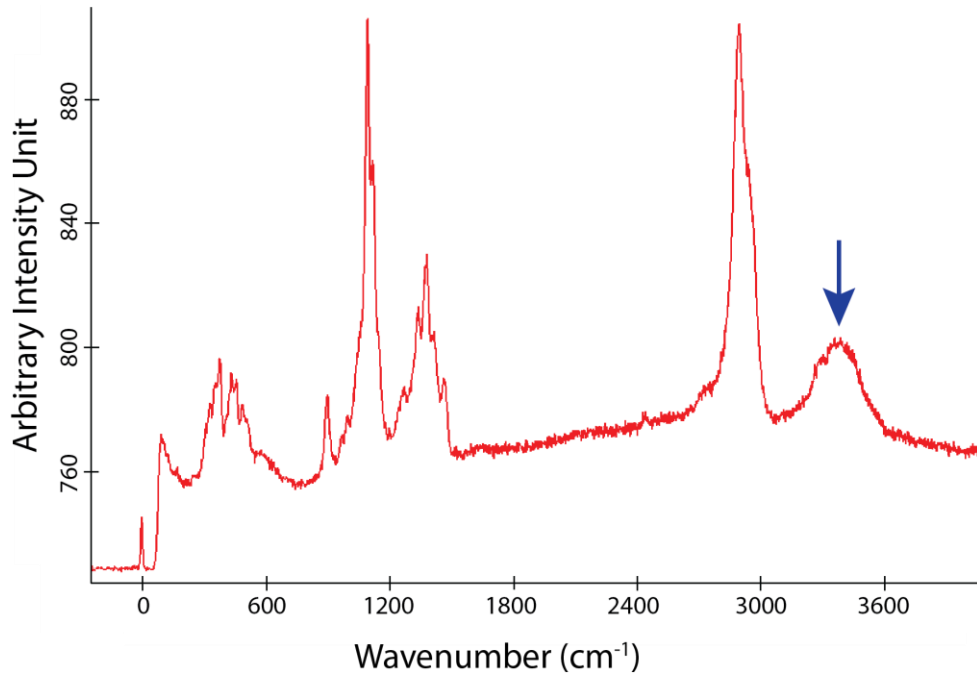
Figure 6 (a-f): SEM images of ash representative ash particles from all eruptions. (a) Novarupta-Katmai, (b) Saint Helens, and (c) Augustine clearly display syn-eruptive and pre-eruptive bubbles, with syn-eruptive bubbles being extremely abundant and closely spaced in the majority of examined particles. (d) Okmok and (e) Spurr also clearly display syn-eruptive and pre-eruptive bubbles, with syn-eruptive bubbles being slightly less abundant and spaced farther apart in the majority of examined particles. (f) Redoubt does not display any syn-eruptive bubbles, only large, pre-eruptive bubble walls are visible in the majority of examined particles.

7.2 Water Content:

We present here preliminary results regarding the presence or absence of water in ash. Ash from Katmai (VEI 6), Saint Helens (VEI 5), Augustine (VEI 4), and Redoubt (VEI 3) all produce spectra indicating the absence of water. Ash from Okmok (VEI 4) and Spurr (VEI 4) both produce spectra suggesting the presence of significant water (**Figures 7a-7b**). It was not feasible in this project to quantitatively derive water content from ash particles due to analytical issues associated with the Micro Raman. This will be further explained in the discussion. There have been no previous studies

employing Micro Raman Spectrometry to confirm or deny the presence of water in ash particles, much less to derive water content of ash particles, therefore this is a preliminary study pointing to a fruitful area for future research.

(a)



(b)

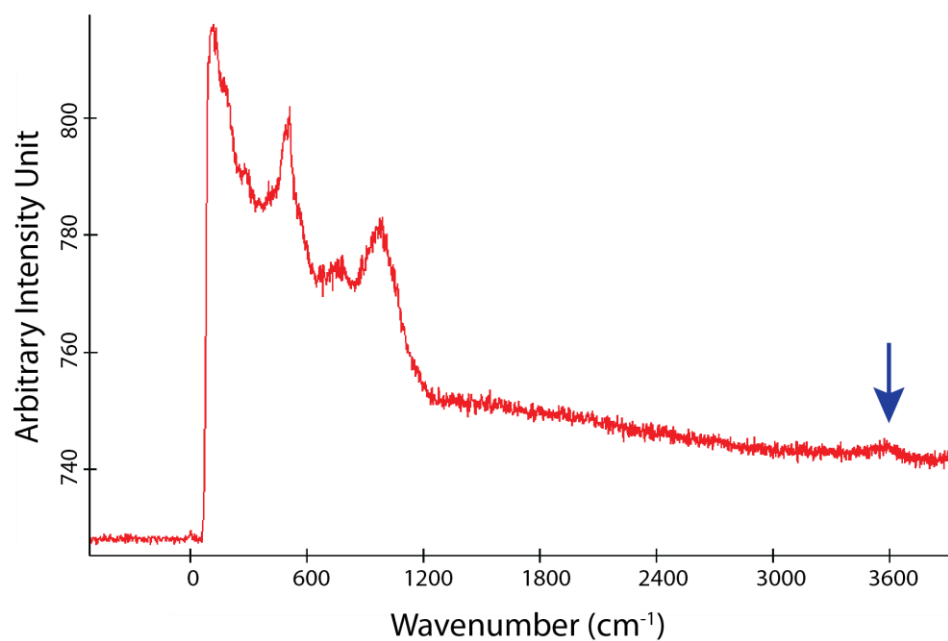
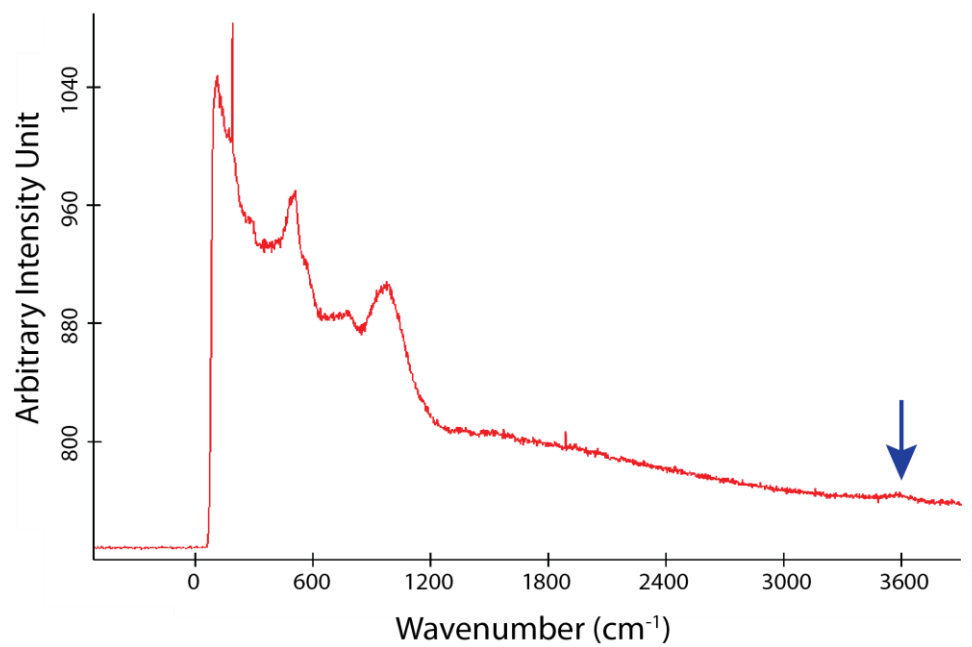


Figure 7 (a-b): Representative Micro Raman Spectra. The location of the peak for water species is represented by the blue arrow. Further explanation of these spectra can be found in **Section 8.2.1**. (a) Okmok spectra. (b) Spurr spectra.

8. Discussion

8.1 Ash Morphology:

8.1.1 Changes in Methodology and Introduction to Conceptual Model:

The initial methodology for this study involved counting the actual number of syn-eruptive and pre-eruptive bubbles that appeared on examined particles. In this way, I would examine the ratio of syn-eruptive to pre-eruptive bubbles, along the reasoning that more energetic eruptions would nucleate more syn-eruptive bubbles and thus would have a higher ratio of syn-eruptive to pre-eruptive bubbles. However, upon beginning the study, I discovered that for all eruptions, among particles from any given eruptions, there were some particles that had syn-eruptive bubbles and others that did not. This means that there are portions of the conduit in which magma was decompressing quickly enough to nucleate syn-eruptive bubbles, as well as portions of the conduit in which decompression was occurring too slowly to allow for the nucleation of syn-eruptive bubbles, because volatiles had time to diffuse into pre-existing bubbles before reaching the critical oversaturation threshold for nucleation. Therefore, I discovered that counting ash particles that contain syn-eruptive bubbles rather than counting syn-eruptive bubbles themselves, allows us to get an idea of the cross-sectional area within the conduit that is decompressing at a sufficiently high rate to nucleate syn-eruptive bubbles. Eruptions with a higher bulk decompression rate have more cross sectional area of magma within the conduit moving at fast enough

rates to nucleate syn-eruptive bubbles. Conversely, eruptions with slower bulk decompression rates have less cross sectional area of magma at the vent moving fast enough to nucleate syn-eruptive bubbles; essentially, comparatively more magma is moving at slow enough rates for volatiles to diffuse into pre-existing bubbles, without the need for a second nucleation event.

In addition to the more conceptually sound basis of using entire ash particles as a means of quantifying syn-eruptive bubble nucleation, rather than numbers of bubbles, there are several logistical reasons for taking this approach. First, it did not seem as if counting individual bubbles would be practically measurable due to analysis limitations. The time-span necessary to count individual bubbles (with hundreds to thousands of syn-eruptive bubbles per particle) would be severely limiting to the number of particles that would be able to be analyzed, which would decrease the sample size significantly and create a less robust sample size for each eruption. Additionally, analysis on a bubble-by-bubble basis would be zooming in to too fine of a scale. In some cases, pre-eruptive bubbles may be too large relative to individual ash particles to be clearly preserved, making it difficult to get a true ratio of syn-eruptive to pre-eruptive bubbles. By looking at only bubble quantities as a basis for the analyses, rather than entire particles, we could perhaps miss the greater picture of conduit processes that is represented in the slightly larger scale of individual ash particles. This is because the particles themselves are representative of magma within the conduit; furthermore, they have the ability to record bubble imprints, and therefore

can describe bubble nucleation processes on magmatic scales which are more representative of eruptive processes as a whole.

In order to combat the issue of the time-consuming bubble-by-bubble analyses, I initially used image analysis software to identify bubbles and therefore eliminate the need to spend manpower and hours manually counting. However, this software, while excellent for purposes such as measuring bubble and particle sizes, is not sufficiently accurate at identifying bubbles. This is because the program identifies features based on their relative darkness and brightness using a grayscale method. As such, unusually dark places on a particle due to a shadow, inclusion, analytical issue capturing the image, etc. could cause the program to overestimate the number of syn-eruptive bubbles. Conversely, anomalously lighter colored bubbles due to the way that the image was captured, risked not being identified as bubbles, and thus underestimating the number of syn-eruptive bubbles. For all of these reasons, conducting this analysis on a particle scale, rather than an individual bubble scale was deemed to be a more robust (and practical) approach.

8.1.2 Katmai:

The understanding of different cross sectional areas being above a critical decompression rate threshold is well illustrated by the studied eruptions. Katmai, with a VEI of 6 (the highest examined in this study) and an SE rating of 79 (also the highest rating found in this study), is not a surprising result. This is because decompression rates in a VEI 6 eruption would have been significantly higher than those associated

with lower VEI eruptions. This is substantiated by the fact that Novarupta-Katmai also had by far the highest plume height, from as low as 17 km to as high as 26 km. The real-time observable evidence that Katmai was the most explosive eruption out of those in this study is sound. The ash tells a similar story to that of VEI and thus plume height. With an SE rating of 79, Katmai had the highest cross sectional area of magma within the conduit ascending at rates fast enough to promote rapid decompression in the vast majority of the conduit. Thus, Katmai's high SE rating is evidence of its high bulk decompression rate.

8.1.3 Saint Helens:

Mt. Saint Helens tells a similar story to Katmai. With a VEI of 5, this had the second highest eruption energy and as such had the second highest plume height (14-24 km). Unsurprisingly, MSH also comes in second for SE rating, with a 69. This indicates that the 1980 eruption of MSH had slightly lower bulk decompression rates than the 1912 eruption of Novarupta-Katmai. As such, slightly less cross-sectional area of magma at the vent overcame the critical decompression rate threshold for the nucleation of syn-eruptive bubbles.

8.1.4 Augustine, Spurr, and Okmok:

VEI 4 eruptions involve several interesting complexities. Augustine Volcano behaves more like a higher VEI eruption, in both plume height and SE rating, coming in just under MSH with a maximum plume height of 16 km and an SE rating of 68. It

is important to note that, while Augustine does differ from other VEI 4 eruptions by having a higher SE rating, it does not differ from the trend of higher plume height and thus decompression rate eruptions producing ash with a higher SE rating, due to more magma being forced above the threshold for the second nucleation to occur. Mt. Spurr and Okmok Volcano both produced ash that yields SE ratings extremely similar to each other, with a 61 and 60, respectively. Both these eruptions had lower plume heights (Okmok max height = 11km, Spurr max height = 15m), than Augustine, which was also a VEI 4, but likely only earned the same VEI assignment as Spurr and Okmok because of its significantly lower eruptive volume. Therefore, it appears as if Spurr, Okmok, and Augustine are all VEI 4 for different reasons; the first two for their relatively high erupted volumes and the last for its relatively high plume height. Since decompression rate is inherently related to plume height and not erupted volume, it makes sense that Spurr and Okmok, with lower plume heights than Augustine, would have lower SE ratings, because of lower bulk decompression rates. While these eruptions erupted more volume total, less of that volume experienced decompression rates necessary to nucleate syn-eruptive bubbles, and thus a lower percentage of ash particles display the remains of syn-eruptive bubbles.

In detail, many particles from Spurr and Okmok display questionable syn-eruptive bubbles. In particles from Novarupta-Katmai, Saint Helens, and Augustine there is very little space between bubbles and thus very thin bubble walls separating individual syn-eruptive bubbles. For this reason, we call the texture found on these particles “honeycomb.” In particles from Spurr and Okmok, there is often quite wide

spacing between ostensibly syn-eruptive bubbles. Because of the relatively wide spacing between bubbles in these eruptions, the texture of these particles resembles “Swiss cheese.” The logical explanation for this is that these two eruptions barely exceed the decompression rate threshold needed to nucleate syn-eruptive bubbles. Because they barely meet required decompression rates, they have less syn-eruptive bubbles, and the syn-eruptive bubbles that did form often did so with difficulty, due to the fact that many remaining volatiles in the melt had enough time to diffuse into pre-existing bubbles. Future studies may focus on quantifying bubble spacing on particles in order to better constrain SE ratings and corresponding decompression rates.

8.1.5 Redoubt:

The lowest VEI eruption examined in this study was Redoubt, with a VEI of 3. Redoubt showed very few particles with syn-eruptive bubbles and correspondingly, a very low SE rating of 7. Redoubt does display some syn-eruptive bubbles, but it is likely that these did not form as a result of high bulk decompression rates, and more likely as the result of localized effects. These localized effects could include turbulence-related, locally high decompression rates in a somewhat energetic plume, or the occurrence of pre-existing bubbles being located so far apart from each other that volatiles did not have time to diffuse into them from the melt before reaching oversaturation, even with very slow decompression occurring. This interpretation is substantiated by the fact that, when the second nucleation occurs, there should be far more syn-eruptive bubbles than pre-eruptive (Genareau et al., 2012). In all other

eruptions in this study, this holds true, and the SE rating is truly representative of cross sectional area of magma decompressing rapidly. Therefore, it is likely that the occurrence of any syn-eruptive bubbles at all in Redoubt is not due to high bulk decompression rates, but is more likely due to localized effects. Bulk decompression rates were insufficiently rapid during this eruption to push a significant portion of the magma over the threshold for the second nucleation to occur. It is therefore concluded that the threshold below which syn-eruptive bubbles cannot form resides between decompression rates associated with VEI 3 and VEI 4 eruptions. It is still unclear exactly where this threshold resides due to vagaries within the VEI scale; in this way, eruptions should be considered energetic based on average plume height. The plume height for Redoubt reached ~18km, but stayed around 10km for the majority of the eruption, indicating that most of the ash investigated in this study would be representative of bulk decompression rates responsible for the average plume height. Better constraining this threshold by comparing these results to other VEI 3 and 4 eruptions remains a fruitful area of study.

8.1.6 Shear in the Conduit as a Conceptual Model:

The differences in SE ratings among eruptions with different energy are related to a continuum of bulk decompression rates, and we interpret this to represent a continuum of cross sectional area of magma that is able to be pushed above the decompression rate necessary for the second nucleation to occur. This continuum is due to shear within the conduit. Decompression rates and flow rate within the conduit

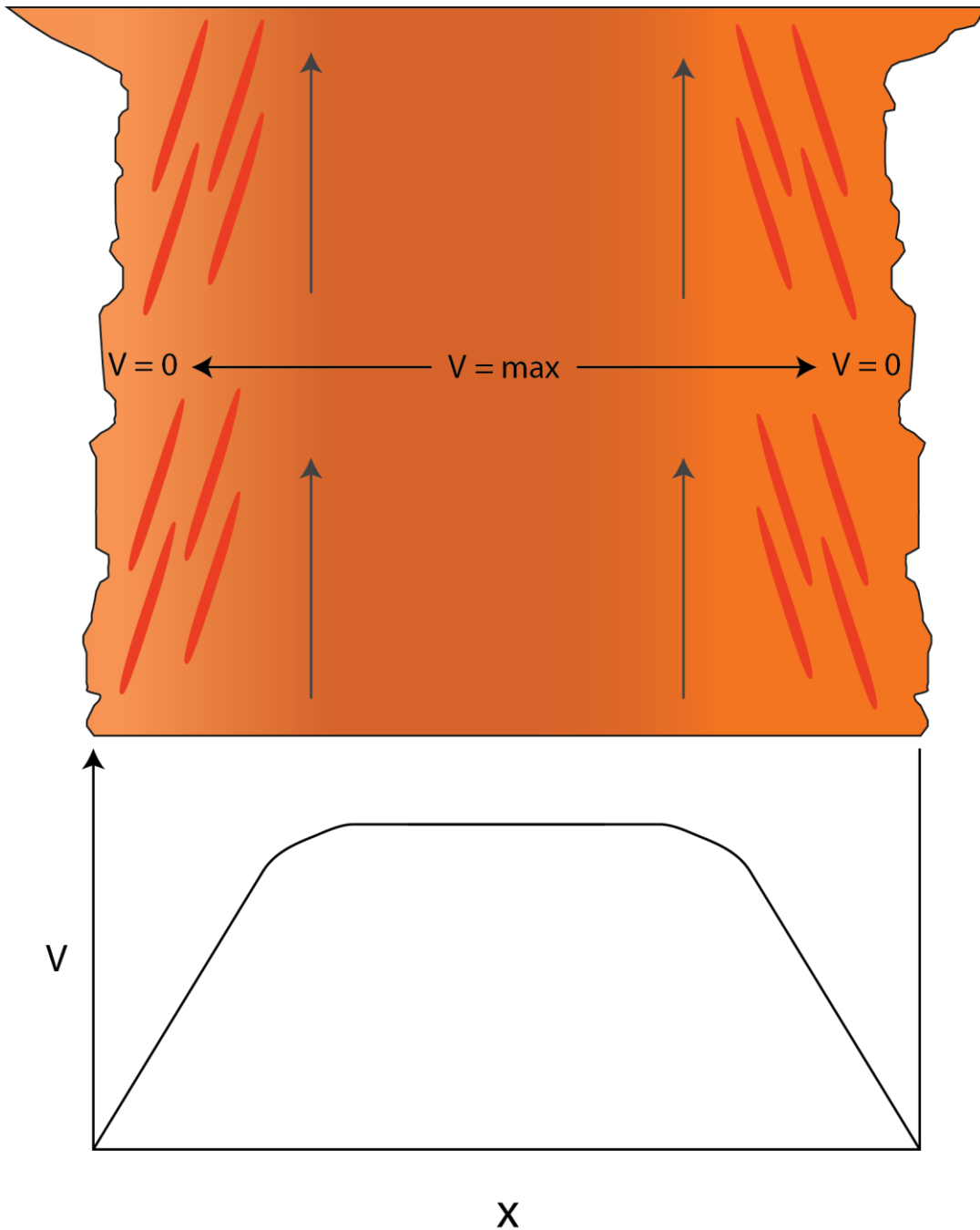


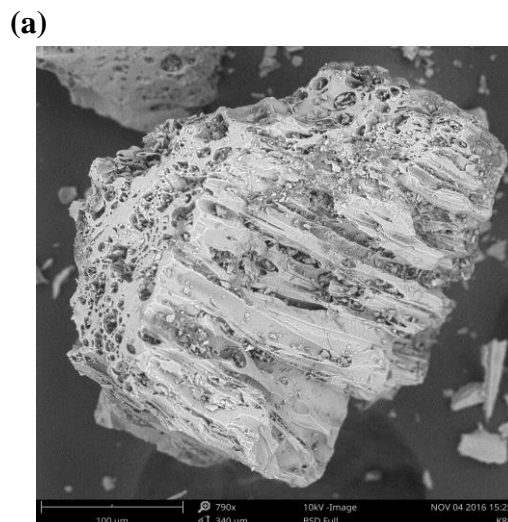
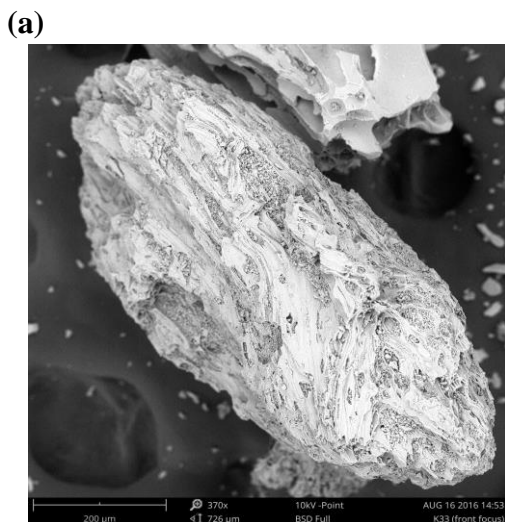
Figure 8: Conceptual diagram of the volcanic conduit during magmatic ascent (vertical direction of magmatic movement indicated by gray arrows). Ascent velocities are highest at the conduit axis and lowest at the walls (indicated by black arrows). Red stretched lines near walls are indicative of likely regions of shear due to the horizontal velocity gradient. The bottom plot shows velocity changes across the conduit, with the steepest velocity gradient occurring near the walls and little to no velocity gradient in the center.

are inherently coupled; as such, higher ascent velocities promote higher decompression rates. Ascent velocities and thus decompression rates are at a maximum in the center of the conduit and zero at conduit walls because the wall rock is not moving and magma in the center of the conduit faces the smallest resistance to vertical flow (Massol et al., 2001). These horizontal velocity differences within the conduit can create a shear zone near the conduit wall where velocity gradients are steepest, within which magma will move slower (**Figure 8**). Therefore, eruptions require high bulk decompression rates to overcome the slowing force of this shear. The higher the bulk decompression rate, the more cross sectional area of magma within the conduit is able to overcome this shear, and the more magma will decompress at rates fast enough to nucleate syn-eruptive bubbles. This conceptual model is my interpretation of varying SE ratings with varying bulk decompression rates. Through this study, I have essentially gained a glimpse within the conduit looking horizontally across, at differential decompression rates and ascent velocities at the point of fragmentation.

8.1.7 Evidence of Shear:

An unexpected result of this study was being able to observe the morphological effects of shear on some ash particles. Novarupta-Katmai had by far the highest number of particles that displayed particle-scale stretching and elongating fabrics that indicate evidence of shear within the conduit (**Figure 9a**). We interpret this to be because Novarupta-Katmai had the highest decompression rates of all the

eruptions. This means that Novarupta-Katmai had very high ascent rates in the center of the conduit, while the wall was still at a velocity of 0. This would create a very large velocity gradient moving from the center to the wall of Novarupta-Katmai during the eruption, which could have manifested itself as a large enough shear zone for our representative sample of ash particles to display numerous sheared particles. This also speaks to the extremely high decompression rate of Novarupta-Katmai; even though there was likely a large shear zone within the conduit which would act as resistance to high ascent velocities, bulk decompression rates were still high enough to push portions of this highly sheared zone above those needed for the second nucleation to occur. Saint Helens and Augustine also contain several particles displaying shear textures, likely also owing to comparatively high decompression rates (**Figures 9b-9c**). Further exploration of this idea should also include an analysis of size and shape of the conduit as well as magma ascent dynamics. This is an interesting area of study, and this study hopes to spark some interest and lend to further investigation of this outstanding question.



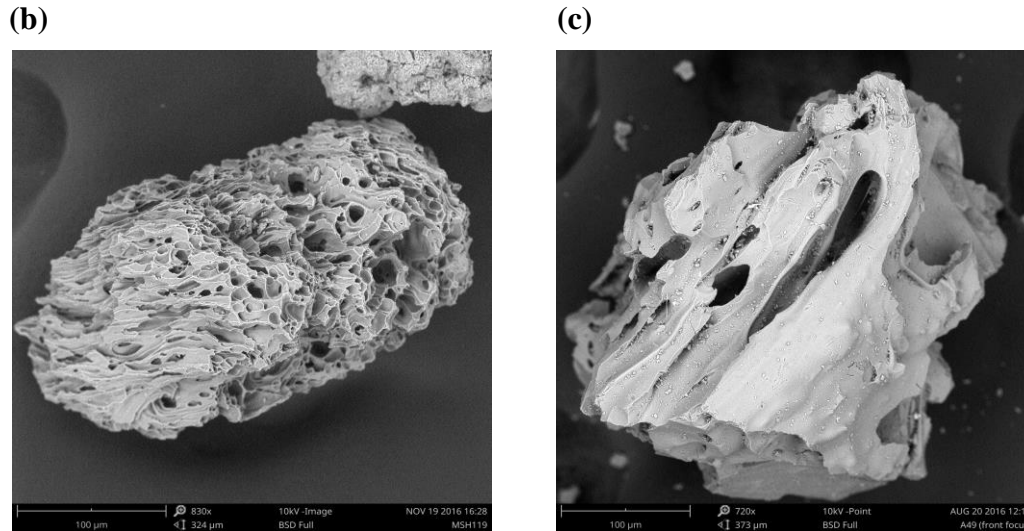


Figure 9 (a-c): SEM images showing sheared particles. (a) Katmai. (b) Saint Helens. (c) Augustine

8.1.8 Sampling Bias:

A question frequently raised in discussion of ash collection is whether or not different sampling locations (mainly distance from the vent) would have an effect on our results. The main factor that collection location would potentially influence could be the size distribution of the particles. Particles examined in this study ranged from ~50-900 μm . Our sample collection location is likely to have contained a temporally and spatially homogenized sample, due to the fact that particles of all sizes (aside from very small particles, which are not of interest in this study of compound ash particles) and produced at all times during the eruption would have been equally likely to fall out of suspension at the points of collection. It is conceivable that the size of the ash particles could affect the likelihood of a particle displaying syn-eruptive and pre-eruptive bubbles, because a smaller ash particle represents a smaller amount of

magma, and thus a smaller space within which syn-eruptive bubbles could have nucleated. However, because during nucleation of syn-eruptive bubbles, the bubbles are far more numerous than pre-eruptive bubbles and account for the vast majority of bubbles in vesicle size distribution analyses, it is unlikely that a complex ash particle would be so small that it would have a lower chance of displaying any syn-eruptive bubbles. Also, syn-eruptive bubbles are very small (10-50 μm) and as such would require an extremely small ash particle to be too small to record syn-eruptive imprints. Particle size often is related to fragmentation depth, as a deeper fragmentation depth will allow for the formation of smaller particles due to collision, leading to comminution and milling in the turbulent plume (Gonnermann, 2015). Because this process occurs post-nucleation and acts on a brittlely fracturing solid incapable of further bubble nucleation, the size of particles should not have any bearing on the likelihood of preserving bubbles.

Furthermore, to check for the possibility of a bias based on particle size, plots were made of the number of particles displaying syn-eruptive bubbles and the number of particles displaying only pre-eruptive particles versus particle size, yielding no correlation (**Appendix 2**). These plots were normalized by dividing each category of particles by the total number of particles of that type for each eruption, and multiplying by 100, in order to get the percentage of the examined particles rather than just the numbers of particles. This is because any trends among particle size and morphology would likely not have been visible in eruptions which had far more of one type of particle than the other. Based on this analysis, we believe that we have fairly

homogenous ash samples, and that any characteristics of these samples did not affect our results.

8.1.9 Effect of Magma Composition:

A commonly raised concern when considering volcanic ash is the potential of compositional variations among eruptions leading to contrasting results because different composition magmas will behave differently in terms of diffusivity, viscosity, etc. If so, the SE ratings derived in this study could have been affected by these differences. Here, I argue that our results would not have been skewed by different compositions, and in fact, compositional differences among eruptions are complementary to these results.

The primary factor affected by compositional differences amongst different magmas would be diffusivity; that is, the ability of water and other volatiles to diffuse through the magma and into the melt during ascent. Bulk water diffusivity increases as silica content decreases; therefore, diffusivity increases from rhyolite to basalt (Behrens et al., 2004). This is a first order approximation of diffusivities based on silica content (Behrens et al., 2004). The eruptions studied here range in composition from andesite to rhyolite (see **Table 1**). For the purposes of this discussion, we compare two end member compositions: andesite, represented by Redoubt (VEI 3) and rhyolite, represented by Novarupta-Katmai (VEI 6).

In an andesitic magma, diffusion rates are higher, allowing for greater diffusion of volatiles from the melt into pre-existing bubbles at depth. This serves to

provide the magma with buoyancy, allowing for high ascent velocities at early stages of the eruption and deep within the conduit. However, by the point of eruption at which syn-eruptive bubbles would be formed, there are less volatiles remaining in the melt due to rapid diffusion early on: with much of the gas already exsolved into bubbles, inter-bubble melt remains below the critical oversaturation level for new bubble nucleation because there is simply less gas remaining in the melt. Therefore, decompression rates at the vent are slower, as there are less volatiles expanding as they change from compressed liquid to gas phase. As such, bulk decompression rates are slower and less magma is pushed above the decompression rate threshold for formation of syn-eruptive bubbles. The higher diffusivity of andesitic magmas allows for greater diffusion at depth, and thus less gas expansion and slower late-stage decompression rates and vent velocities upon eruption (**Figure 10**).

Conversely, rhyolite is highly viscous and as such has slower diffusion rates. Volatiles remain trapped in the melt and do not as readily diffuse into pre-existing bubbles at depth. Also, rhyolite tends to have higher initial volatile content than the less silicic magmas. These circumstances result in extreme oversaturation of the melt in late-stages of ascent; such high supersaturation allows for extremely high bubble nucleation rates (Gonnermann & Gardner, 2013). Such a high gas volume causes catastrophic expansion of the gassy foam upon eruption, resulting in extremely high decompression rates. As such, bulk decompression rates are higher and more cross sectional area of the magma is pushed over the threshold for the formation of syn-eruptive bubbles. Slow diffusivity of rhyolite at depth allows for less diffusion at

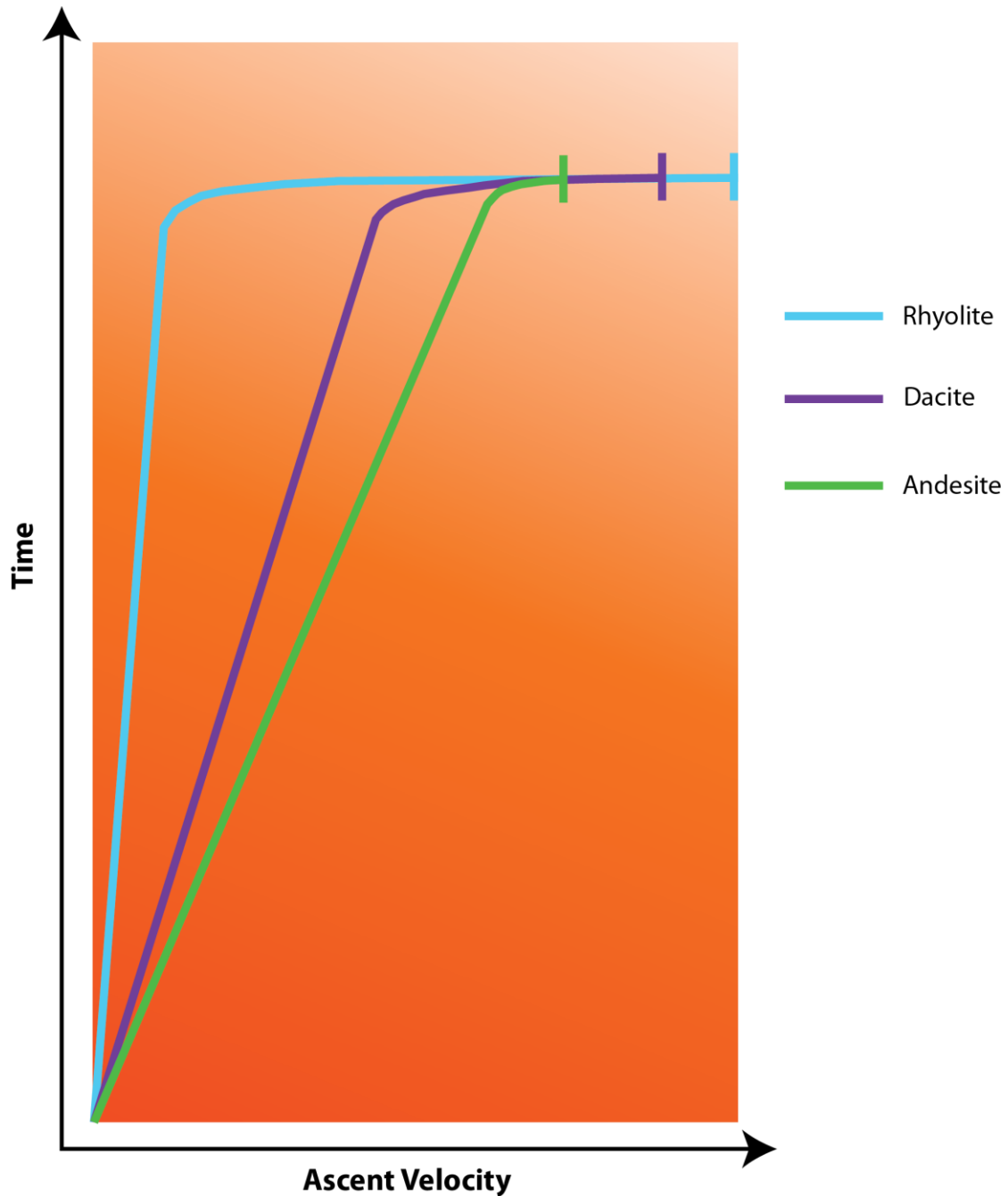


Figure 10: Generalized plot of time versus ascent velocity for magmas of various compositions. Andesite, because of higher diffusivity, has greater bubble growth and depth (5-8km), allowing for fairly rapid ascent at depth, but a volatile-depleted melt upon eruption, causing little late-stage increase in velocity and ultimately slower final ascent velocities and eruption rates. Conversely, rhyolite, because of lower diffusivity, has less bubble growth at depth, allowing for fairly slow ascent velocities at depth, but great supersaturation upon eruption, causing a large late-stage increase in velocity and ultimately higher ascent velocities and eruption rates.

depth, greater late-stage supersaturation in the melt, and thus more gas expansion and higher late-stage decompression rates and vent velocities upon eruption (**Figure 9**).

Different diffusivities would be of consequence at earlier stages of an eruption, during which pre-eruptive bubbles are forming and growing via diffusion of volatiles out of the melt. However, syn-eruptive bubbles are formed extremely late-stage, just before fragmentation, as indicated by coinciding peak bubble, nucleation, and fragmentation overpressures (Gonnermann & Houghton, 2012). At the point of fragmentation, small fragments of magma that become ash behave as solids (Genareau, 2013). This is indicated by the lack of bulges within ash particles, which would indicate continued expansion of gasses into a viscous liquid after fragmentation (Genareau, 2013). Because of this solid behavior, it is clear that diffusion stops at the point of fragmentation, and thus the size distributions of bubbles preserved in ash are not affected by late-stage, post-fragmentation diffusion processes. Therefore, diffusivity differences effect magma in the early stages of ascent, but do not skew the relationship established here between explosivity and syn-eruptive bubble formation; this process is truly dictated by decompression rates at the vent upon fragmentation.

Furthermore, because composition has a strong control on decompression rate, and we seek to compare eruptions of various decompression rates to the physical and chemical properties preserved in ash particles, it was necessary for us to select eruptions with a range of compositions. We are only interested in truly explosive eruptions, so we use andesitic eruptions as the lowest silica content end member, and primarily rhyolitic eruptions as the high silica end member. In this way, we are able to

observe the behavior of bubbles and water in ash particles from a range of explosivities, in order to develop a relationship between ash morphology and explosivity, and thus establish this method as a new tool with which we can understand eruption energetics and forecast possible hazards.

8.2 Water Content:

8.2.1 Problems with Micro Raman Spectroscopy:

This study presents the first attempted use of Micro Raman Spectrometry to derive chemical constituents of ash particles. The size and topography of individual ash particles, combined with the complexities of the Micro Raman spectrometer, presented challenges for such exploratory efforts. The Micro Raman is severely limited in its depth of field capabilities. As such, it was impossible to focus on an entire particle at any one time, and extremely difficult to focus on even a small section of a particle, given that ash particles have significant topography and are very rarely flat along any considerable portion of surface area. This proved to be an intense challenge while working with this instrument; it was initially thought that we might try to determine water concentrations moving to and from pre-eruptive bubble walls, but the lack of ability to focus on large parts of the particle made it impossible to identify bubble walls with any certainty. For the same reason, it was also impossible to identify any syn-eruptive bubbles on the particles using the imaging feature of the microscope, which eliminated the determination of a possible correlation between the

presence or absence of syn-eruptive bubbles and the amount of water contained within those particles. At times, we were not even sure if what we were imaging was an ash particle or some sort of mineral or lithic fragment. In these cases, we either confirmed or denied that the sample was an ash particle based on the presence or absence of produced spectra containing characteristic wavelength shifts associated with bridging tetrahedron-oxygen-tetrahedron linkages (Si or Ti) and non-bridging tetrahedron-oxygen linkages (Si, Ti, Al, Fe). These characteristic wavelengths make up the 200-1200 cm^{-1} wavenumber of the spectra, which represents the aluminosilicate framework region (ASF) (Shea, 2016). Peaks in this region of the spectra must be present in order for the sample to be an ash particle because an ash particle from these eruptions would certainly contain bonded silica.

Initial analysis using the Micro Raman was problematic and refinement of the technique will be necessary before it can be effectively utilized for future studies. However, the perceived presence or absence of water in ash is an interesting result on its own. The data outlined in the results is intriguing nevertheless and will be discussed in more detail below, while keeping in mind the possible analytical limitations involved with using this instrument for this purpose.

8.2.2. Spurr and Okmok:

The presence of water in Okmok and Spurr and lack thereof in all other examined eruptions is initially a surprising result, given that Spurr and Okmok are of intermediate VEI, plume height, and SE rating. However, it is not surprising that Spurr

and Okmok behave similarly in terms of water content because they are extremely similar in all other eruption characteristics. They have similar plume height and erupted volumes, are the same VEI, and produce nearly negligibly different SE ratings (Spurr has an SE rating of 60 while Okmok has an SE rating of 61). The presence of water remaining in these glasses upon eruption could be a glimpse into the time-limited nature of the diffusion of water through magma and into bubbles. We interpret the presence of water in particles of Okmok and Spurr and its notable absence in particles from all other eruptions to have occurred because these two eruptions rest in a sort of middle ground of decompression rates. Unlike Redoubt, they both had bulk decompression rates high enough to force the majority of magma within the conduit over the decompression rate threshold for nucleation of syn-eruptive bubbles. However, both of these eruptions had noticeably lower SE ratings than Augustine, St. Helens, and Katmai (SE ratings of 68, 69, and 70, respectively). Therefore, Spurr and Okmok created less syn-eruptive bubbles than these eruptions.

Furthermore, syn-eruptive bubbles in Spurr and Okmok are spaced more widely apart than in Augustine, St. Helens, and Katmai. Spurr and Okmok particles display a “Swiss cheese” pattern of syn-eruptive bubbles and interstitial glass, while Augustine, St. Helens, and Katmai display more of a “honeycomb” pattern of syn-eruptive bubbles and interstitial glass. Based on the less common occurrence of syn-eruptive bubbles, it could have been that, upon eruption, magma ascent rates were sufficiently rapid to nucleate some syn-eruptive bubbles, but not rapid enough to force all magmatic water to nucleate. Given the wider spacing of syn-eruptive bubbles in

Spurr and Okmok eruptions, magmatic water would have had more distance to travel before reaching a bubble to diffuse into, and thus became locked in interstitial glass upon fragmentation. This interpretation is certainly open for discussion and scrutiny, given the difficulties of using Micro Raman for this purpose. It is possible that there is water in other eruptions as well and that our relatively small sample size and other analytical difficulties did not allow for its detection. However, considering the similarities between every other facet of the Spurr and Okmok eruptions, we do believe that both molecular water and hydroxyl groups would behave similarly between the two, and that this is indeed a real result and not an analytical artifact.

8.2.3 Novarupta-Katmai:

The lack of water in analyses of Novarupta-Katmai ash is interesting given the findings of other studies that predicted that, by the time fragmentation occurred in this highly explosive eruption, Katmai had only lost ~10-20% of dissolved magmatic volatile (Gonnermann & Houghton, 2012). This indicates one of two things: 1. Katmai still has a large portion of magmatic water retained in the glass or 2. Open-system degassing of volatiles from the magma occurred aggressively in the time period between fragmentation and quenching (Gonnermann & Houghton, 2012). Given our preliminary results that indicate an absence of water in Katmai ash, this study suggests the latter of those two options. It is beyond the scope of this study to further explore the mechanisms or implications of that conclusion, but more work is certainly needed

in that area, potentially involving the use of hydrogen isotopes to explore degassing and open-system behavior.

8.2.4 Presence of Water in Ash:

It is interesting that any water in ash can be detected given that ash is produced from the most energetic phase of an eruption during which oversaturation and bubble nucleation would have been at its highest. Other studies suggest that magma loses much of its dissolved water upon eruption. One such study suggests that magmas only contained 0.2 - 0.5 wt% of magmatic water upon eruption, suggesting that the magma was nearly dry by the time it erupted (Giachetti et al., 2015). This is clearly an area that requires further attention, and is an intriguing portion of this study.

9. Conclusions

- Based on bubble nucleation processes in magma upon eruption, bubble imprints preserved in ash particles provide useful proxies that can be used to determine the relative explosivity of an eruption. This is extremely useful given the limitations of the Volcanic Explosivity Index in estimating explosivities of pre-historic or poorly studied eruption. This study provides a tool by which volcanologists can better characterize the explosivities of past eruptions in order to more accurately predict explosivities of future eruptions and improve volcanic hazard prediction and preparedness.

- It is possible to observe the threshold below which syn-eruptive bubbles do not form, as represented by VEI 3 eruptions. Redoubt, VEI 3, has an SE rating of 7, meaning that bulk decompression rates were much lower than higher VEI eruptions and as such, volatiles had sufficient time to diffuse into pre-existing bubbles rather than nucleate syn-eruptive bubbles. Any syn-eruptive bubbles observed in ash from Redoubt likely are the result of locally high decompression rates in more turbulent portions of the plume.
- More particles displaying syn-eruptive bubbles can be observed in higher energy eruptions relative to lower energy eruptions. Katmai, VEI 6, had an SE rating of 79 and Spurr, VEI 4, had an SE rating of 60. Okmok, Augustine, and Saint Helens all had SE ratings falling between 60 and 79, and correlating positively with increasing energy. This is because eruptions with higher bulk decompression rates are capable of pushing a larger cross sectional area of magma over the threshold for the nucleation of syn-eruptive bubbles.
- A horizontal velocity gradient exists within the conduit and creates shear zones near the conduit wall. The higher the maximum ascent velocity for the eruption, the larger the shear zone. Novarupta-Katmai, with extremely high ascent velocities, has a larger number of particles that display a sheared texture. Saint Helens and Augustine, also high-energy eruptions, have several particles displaying a shear texture as well.
- Water content is difficult to measure, but there does appear to be water remaining in Okmok and Spurr, both intermediate-energy eruptions. This indicates

that corresponding decompression rates allow for the nucleation of syn-eruptive bubbles, but not complete supersaturation of all water species in the magma at the time of fragmentation. Bubble spacing in Okmok and Spurr also likely contributes to the existence of water within ash; bubbles were spaced too far apart for magmatic water to diffuse into them upon rapid decompression.

- These morphological and chemical results are an important step in better understanding the mechanisms that drive highly energetic volcanic eruptions, and therefore can provide the basis for improved volcanic ash behavior models, which have a direct impact on the health, safety, and economies of the world, especially in regions where volcanism is persistent. This study takes a step towards bridging the gap in understanding of eruption mechanisms and eruptive products, and is thus useful in the reconstruction of pre-historic eruption energies, in order to inform potential risks posed by explosive eruptions in the future.

10. Recommendations for Future Research

This study raised many interesting question in regards to conduit dynamics as they relate to conduit geometry. Clearly, there are velocity gradients, which contribute to shear within the conduit, but the extent to which this shear is influenced by other factors such as conduit size and shape is yet to be determined. Future studies may further explore the controls on shear within the conduit and what type of effect this

could have on eruption energetics, as well as how shear is manifested in eruptive products.

Water content in ash particles is also an intriguing area of study that requires further work. This study presents preliminary data from Micro Raman Spectroscopy that indicate the presence of water in some ash particles. This is an intriguing result as it suggests that volatiles are still present in the melt even after the most explosive eruptive phase. Something else that should be explored further is exactly how bubble spacing and geometry affects the presence of water remaining in ash particles. Additionally, it was not possible to directly calculate water concentrations from ash particles, but this remains of utmost importance in order to fully understand volatile behavior in eruptions, and to make the link between magmatic water preserved in ash particles and eruption explosivity. Future studies might consider exploring new methods with which water can be measured from ash particles. These new methods should be capable of detecting water at very fine scales, but not so sensitive that ash particle topography complicates the procedure. The Micro Raman technique needs some fine tuning and shows great potential for measuring water concentration gradients throughout ash particles. Water concentration gradients moving away from bubble walls could shed light on the behavior of water at the point of eruption, as well as further explore the concept of resorption from bubbles back into the melt.

It is clear that the threshold above which syn-eruptive bubbles can nucleate resides in between VEI 3 and 4 eruptions. Future studies may better constrain this threshold by comparing these results to other VEI 3 and 4 eruptions, making sure to

take into account eruption specifics such as plume height. This comparison will not only add to this dataset, but also come closer to truly identifying the critical decompression rate threshold for the nucleation of syn-eruptive bubbles.

The SE Rating provides an innovative approach to understand horizontal velocity gradients within the volcanic conduit. Through this rating, it is clear that a trend exists between eruption energy and syn-eruptive bubble nucleation. However, in order to better constrain this relationship, future studies could build into the SE Rating a quantitative measure of particle texture that accounts for characteristics such as bubble spacing. This study qualitatively describes textural phenomena, but quantification of bubble spacing remains an important step in order to better constrain the relationship between ash morphology and syn-eruptive bubbles. This quantification could potentially be done using SEM imaging and image analysis software to identify spacing. It could also be done by measuring porosity and permeability of ash particles to learn about the distribution of voids representing bubbles. This is an interesting area of potential work that can build upon the results presented here.

Lastly, numerical modeling of conduits should be updated to reflect the nucleation of syn-eruptive bubbles, as well as the feedback of nucleation with decompression. Proussevitch and Sahagian (1996, 1998) and Sahagian and Proussevitch (2005) develop a series of numerical models describing bubble growth and diffusion in the magma chamber as an eruption occurs. These models describe some of the processes that control bubble growth within the conduit as the eruption

progresses. Future models such as these should include the second nucleation event in order to properly describe the feedback between this event and the acceleration of decompression rates. Future models could scale the magnitude of this feedback to the relative volume of magma above the decompression rate threshold for formation of syn-eruptive bubbles to better determine how eruptions of various explosivities are affected by the magnitude of syn-eruptive bubble nucleation.

REFERENCES

- Andronico, D., Del Carlo, P. (2016). PM10 measurements in urban settlements after lava fountain episodes at Mt. Etna, Italy: Pilot test to assess volcanic ash hazard to human health. *Natural Hazards and Earth System Science*, 16(1), 29-40.
<http://dx.doi.org/10.5194/nhess-16-29-2016>
- Baldini, J.U.L., Brown, R.J., McElwain, J.N. (2015). Was millennial scale climate change during the Last Glacial triggered by explosive volcanism? *Scientific Reports*, 5, 1-9. <http://dx.doi.org/10.1038/srep17442>
- Behrens, H., Zhang, Y., Xu, Z. (2004). H₂O diffusion in dacitic and andesitic melts. *Geochimica et Cosmochimica Acta*, 68(24), 5139-5150.
<http://doi.org/10.1016/j.gca.2004.07.008>
- Carey, R.J., Sigurdsson, H., Gardner, J.E., Criswell, W. (1990). Variations in column height and magma discharge during the May 18, 1980 eruption of Mt. Saint Helens. *Journal of Volcanology and Geothermal Research*, 43, 99-112.
[https://doi.org/10.1016/0377-0273\(90\)90047-J](https://doi.org/10.1016/0377-0273(90)90047-J)
- Casadavall, T. (1994). The 1989-1990 eruption of Redoubt Volcano, Alaska – Impacts on aircraft operations. *Journal of Volcanology and Geothermal Research*, 62, 301-316. [https://doi.org/10.1016/0377-0273\(94\)90038-8](https://doi.org/10.1016/0377-0273(94)90038-8)
- Criswell, C.W. (1987). Chronology and pyroclastic stratigraphy of the May 18, 1980 eruption of Mount St. Helens, Washington. *Journal of Geophysical Research*, 92(B10), 10,237-10,266. <https://doi.org/10.1029/JB092iB10p10237>
- Dunbar, N.W., Kyle, P.R. (1992). Volatile contents of obsidian clasts in tephra from the Taupo Volcanic Zone, New Zealand: Implications to eruptive processes. *Journal of Volcanology and Geothermal Research*, 49(1-2), 127-145.
[https://doi.org/10.1016/0377-0273\(92\)90009-3](https://doi.org/10.1016/0377-0273(92)90009-3)
- Eichelberger, J.C., Terry, E.C., Miller, T.P., Nye, C.J., (1992). The 1992 Eruptions of Crater Peak Vent, Mount Spurr Volcano, Alaska: Chronology and Summary. *U.S. Geological Survey Bulletin*, 2139.
- Fierstein, J., Hildreth, W. (1992). The plinian eruptions of 1912 at Novarupta, Katmai National Park, Alaska. *Bulletin of Volcanology*, 54(8), 646-84.
<https://doi.org/10.1007/BF00430778>
- Fruchter, J.S., Robertson, D.E., Evans, J.C., Olsen, K.B., Lepel, E.A., Laul, J.C., Abel, K.H., Sanders, R.W., Jackson, P.O., Wogman, N.S., Perkins, R.W., Van Tuyl, H.H., Beauchamp, R.H., Shade, J.W., Daniel, J.L., Erikson, R.L., Sehmel, G.A., Lee,

- R.N., Robinson, A.V., Moss, O.R., Briant, J.K., Cannon, W.C. (1980). Mount St. Helens ash from the 18 May 1980 eruption: chemical, physical, mineralogical, and biological properties. *Science*, 209(4461), 1116-25.
<https://doi.org/10.1126/science.209.4461.1116>
- Genareau, K., Proussevitch, A.A., Durant, A.J., Mulukutla, G., Sahagian, D.L. (2012). Sizing up the bubbles that produce very fine ash during explosive volcanic eruptions. *Geophysical Research Letters*, 39, LI15306.
<https://doi.org/10.1029/2012GL052471>
- Genareau, K., Mulukutla, G.K., Proussevitch, A.A., Durant, D.J., Rose, W.I., Sahagian, D.L. (2013). The size range of bubbles that produce ash during explosive volcanic eruptions. *Journal of Applied Volcanology, Society and Volcanoes*, 2(4), 1-18. <https://doi.org/10.1186/2191-5040-2-4>
- Giachetti, T., Gonnermann, H.M. (2013). Water in volcanic pyroclast: Rehydration or incomplete degassing? *Earth and Planetary Science Letters*, 369-370, 317-332.
<http://doi.org/10.1016/j.epsl.2013.03.041>
- Global Volcanism Program (2008). Report on Okmok (United States). *Bulletin of the Global Volcanism Network*, 33, 7.
<http://dx.doi.org/10.5479/si.GVP.BGVN200807-311290>
- Graham, J., Miller, F., Davies, D., Hiteshew, M., Walsh, L. (1985). Inhalation studies of Mt. St. Helens volcanic ash in animals, 1. Introduction and exposure system. *Environmental Research*, 37, 61-71.
[http://dx.doi.org/10.1016/0013-9351\(85\)90049-0](http://dx.doi.org/10.1016/0013-9351(85)90049-0)
- Gonnermann, H.M. (2015). Magma Fragmentation. *Annual Review of Earth and Planetary Science*, 43, 431-58.
<http://dx.doi.org/10.1146/annurev-earth-060614-105206>
- Gonnermann, H.M. Houghton, B.F. (2012). Magma degassing during the Plinian eruption of Novarupta, Alaska, 1912. *Geochemistry, Geophysics, Geosystems*, 13(10), 1-20. <http://dx.doi.org/10.1029/2012GC004273>
- Gonnermann, H.M, Gardner, J.E. (2013). Homogenous bubble nucleation in rhyolitic melt: Experiments and nonclassical theory. *Geochemistry, Geophysics, Geosystems*, 14(11), 4758-4773. <http://dx.doi.org/10.1002/ggge.20281>
- Hervig, R.L., Dunbar, N. Westrich, H.R., Kyle, P.R. (1989). Pre-eruptive water content of rhyolitic magmas as determined by ion microprobe analyses of melt inclusions in phenocrysts. *Journal of Volcanology and Geothermal Research*, 36(4), 293-302. [https://doi.org/10.1016/0377-0273\(89\)90075-9](https://doi.org/10.1016/0377-0273(89)90075-9)

- Hildreth, W., Fierstein, J. (2012). The Novarupta-Katmai eruption of 1912 – largest eruption of the twentieth century; centennial perspectives. *United States Geological Survey Professional Paper, 1791*.
- Horwell, C.J., Sparks, R.S.J., Brewer, T.S., Llewellyn, E.W., Williamson, B.J. (2003). Characterization of respirable volcanic ash from the Soufriere Hills volcano, Montserrat, with implications for human health hazards. *Bulletin of Volcanology*, 65(5), 346-362. <https://doi.org/10.1007/s00445-002-0266-6>
- Johnston, D., Stewart, C., Leonard, G.S., Hoverd, J., Thordarsson, T., Cronin, S. (2004). Impacts of volcanic ash on water supplies in Auckland: Part I. *Institute of Geological & Nuclear Sciences Science Report, 25*.
- Koyaguchi, T. (2005). An analytical study of 1-dimensional steady flow in volcanic conduits. *Journal of Volcanology and Geothermal Research*, 143(1-3), 29-52. <http://doi.org/10.1016/j.jvolgeores.2004.09.009>
- Larsen, J.F. (2016). Unraveling the diversity in arc volcanic eruption styles: Examples from the Aleutian volcanic arc, Alaska. *Journal of Volcanology and Geothermal Research*, 327, 643-668. <http://doi.org/10.1016/j.jvolgeores.2016.09.008>
- Larsen, J.F., Sliwinsky, M.G., Nye, C., Cameron, C., Schaefer, J.R. (2013). The 2008 eruption of Okmok Volcano, Alaska: petrological and geochemical constraints on the subsurface magma plumbing system. *Journal of Volcanology and Geothermal Research*, 264, 85-105. <http://doi.org/10.1016/j.jvolgeores.2013.07.003>
- Massol, H., Koyaguchi, T. (2005). The effect of magma flow on nucleation of gas bubbles in a volcanic conduit. *Journal of Volcanology and Geothermal Research*, 143, 69-88. <http://doi.org/10.1016/j.jvolgeores.2004.09.011>
- Massol, H., Jaupart, C., Pepper, D.W. (2001). Ascent and decompression of viscous vesicular magma in a volcanic conduit. *Journal of Geophysical Research: Solid Earth*, 106(B8), 16223-16240. <http://doi.org/10.1029/2001JB000385>
- McIntosh, I.M., Llewellyn, E.W., Humphreys, M.C.S., Nichols, A.R.L., Burgisser, A., Schipper, C.I., Jarsen, J.F. (2014). Distribution of dissolved water in magmatic glass records growth and resorption of bubbles. *Earth and Planetary Science Letters*, 401, 1-11. <http://doi.org/10.1016/j.epsl.2014.05.037>
- Neal, C.A., McGimsey, R.G., Garder, C.A., Harbin, M.L., Nye, C.J. (1995). Tephra-fall deposits from the 1992 eruptions of the Crater Peak, Mount Spurr volcano, Alaska: a preliminary report on distribution, stratigraphy, and composition. *USGS Bulletin, 2139*, 65-79

- Newhall, C.G., Self, S. (1982). The Volcanic Explosivity Index (VEI): An Estimate of Explosive Magnitude for Historical Volcanism. *Journal of Geophysical Research*, 87(C2), 1231-1238. <http://doi.org/10.1029/JC087iC02p01231>
- Pistone, M., Cordonnier, B., Ulmer, P., Caricchi, L. (2016). Rheological flow laws for multiphase magmas: An empirical approach. *Journal of Volcanology and Geothermal Research*, 321, 158-170. <http://doi.org/10.1016/j.jvolgeores.2016.04.029>
- Prata A. and Tupper, A. (2009). Aviation hazards from volcanoes: The state of science. *Natural Hazards*, 51, 239-244. <http://doi.org/10.1016/10.1007/s11069-009-9415-y>
- Proussevitch, A.A., Sahagian, D.L. (1993). Stability of foams in silicate melts. *Journal of Volcanology and Geothermal Research*, 59(1-2), 161-178. [https://doi.org/10.1016/0377-0273\(93\)90084-5](https://doi.org/10.1016/0377-0273(93)90084-5)
- Proussevitch, A.A., Sahagian, D.L. (1996). Dynamics of coupled diffusive and decompressive bubble growth prior to volcanic eruption. *Journal of Geophysical Research*, 101(B8), 17,447-17,255. <https://doi.org/10.1029/96JB01342>
- Proussevitch, A.A., Sahagian, D.L. (1998). Dynamics and energetics of bubble growth in magmas: analytical formulation and numerical modeling. *Journal of Geophysical Research*, 103(B8), 18,223-18-251. <https://doi.org/10.1029/98JB00906>
- Robock, A. (2000). Volcanic eruptions and climate. *Reviews of Geophysics*, 38, 191-219. <https://doi.org/10.1029/1998RG000054>
- Sahagian, D.L. (1999). Volcanology: Magma fragmentation in eruptions. *Nature*, 402, 589-591. <https://doi.org/10.1038/45099>
- Sahagian, D.L., Proussevitch, A.A. (1998). 3D particle size distributions from 2D observations: stereology for natural applications. *Journal of Volcanology and Geothermal Research*, 84, 173-196. [http://doi.org/10.1016/S0377-0273\(98\)00043-2](http://doi.org/10.1016/S0377-0273(98)00043-2)
- Sahagian, D.L., Proussevitch, A.A. (2005). Standardized mode runs and sensitivity analysis using the “Bubbledrive-1” volcanic conduit flow model. *Journal of Volcanology and Geothermal Research*, 143(1-3), 173-185. <http://doi.org/10.1016/j.jvolgeores.2004.09.016>
- Santer, B.D., Bonfils, C., Painter, J.F., Zelinka, M.D., Mears, C., Solomon, S., Schmidt, G.A., Fyfe, J.C., Cole, J.N.S., Nazarenko, L., Taylor, K.E., Wentz, F.J. (2014). Volcanic contribution to decadal changes in tropospheric temperature.

Nature Geoscience, 7, 185-189. <http://doi.org/10.1038/ngeo2098>

Sarna-Wojcicki, A.M., Shipley, S., Waite Jr., R.B., Dzurisin, D., Wood, S.H. (1981). Areal distribution, thickness, mass, volume, and grain-size of air-fall ash from the six major eruptions of 1980. *United States Geological Survey Professional Paper*, 1250, 577-600

Shea, T. (2016). Quantification of water in glasses using microRaman analysis. Retrieved from <http://www.soest.hawaii.edu/GG/FACULTY/tshea/raman.html>

Stewart, C., Pizzolon, L., Wilson, T., Leonard, G., Dewar, D., Johnston, D., Cronin, S. (2009). Can volcanic ash poison water supplies? *Integrated Environmental Assessment and Management*, 5(4), 713-716. http://doi.org/10.1897/IEAM_2009-062.1

Toramaru, A. (2006). BND (bubble number density) decompression rate meter for explosive volcanic eruptions. *Journal of Volcanology and Geothermal Research*, 154, 303-316. <http://doi.org/10.1016/j.jvolgeores.2006.03.027>

Toramaru, A. (2014). On the second nucleation of bubbles in magmas under sudden decompression. *Earth and Planetary Science Letters*, 404, 190-99. <http://doi.org/10.1016/j.epsl.2014.07.035>

Tsuya, H. (1955). Geological and petrological studies of volcano Fuji. *Tokyo Daigaku Jishin Kenkyusho Iho*, 5(33), 341-382.

Wallace, K.L., Neal, C.A., McGimsey, R.G. (2010). Timing, distribution, and character of tephra fall from the 2005-2006 eruption of Augustine Volcano. *USGS Professional Paper*, 1769, 187-217.

Wallace, K.L., Schaefer, J.R., Coombs, M.L. (2013). Character, mass, distribution, and origin of tephra-fall deposits from the 2009 eruption of Redoubt Volcano, Alaska – Highlighting the significance of particle aggregation. *Journal of Volcanology and Geothermal Research*, 259, 145-69. <http://doi.org/10.1016/j.jvolgeores.2012.09.015>

Wilson, T.M., Stewart, C., Sword-Daniels, V., Leonard, G.S., Johnston, D.M., Cole, J.W., Wardman, J., Wilson, G., Barnard, S.T. (2011). Volcanic ash impacts on critical infrastructure. *Physics and Chemistry of the Earth*, 45, 5-23. <http://doi.org/10.1016/j.pce.2011.06.006>

Zhang, Y. (199). A criterion for the fragmentation of bubbly magma based on brittle fracture theory. *Nature*, 402, 648-650. <http://doi.org/10.1038/45210>

APPENDICES

Appendix 1: Raw ash morphology data and SE ratings obtained from SEM observation.

Redoubt:

Particle #	Particle Size (µm)	Two Populations (0 if only PE, 1 if PE and SE)
R1	180	0
R2	215	0
R3	229	0
R4	167	0
R5	112	0
R6	371	0
R7	95.4	0
R8	114	0
R9	145	0
R10	257	0
R11	176	0
R13	82	0
R14	558	0
R15	57	0
R16	222	0
R17	651	0
R18	334	0
R19	253	0
R20	222	0
R21	233	0
R22	347	0
R23	313	0
R24	182	0
R25	153	1
R27	628	0
R28	435	0
R29	248	0
R30	340	0
R31	418	1
R32	311	0

Particle #	Particle Size (µm)	Two Populations (0 if only PE, 1 if PE and SE)
R33	303	0
R34	146	0
R35	360	0
R36	315	0
R37	238	0
R38	191	0
R39	325	0
R40	304	0
R41	501	0
R42	400	0
R43	480	0
R44	475	0
R45	352	0
R46	262	0
R47	476	0
R48	276	0
R49	304	0
R50	367	0
R51	136	0
R52	273	0
R53	206	0
R54	108	0
R55	169	0
R56	114	0
R57	52.4	0
R58	167	0
R59	79.3	0
R60	111	0
R61	174	0
R62	186	0
R63	92.8	0
R64	110	0
R66	411	0
R67	396	1
R68	91.2	1
R69	124	0
R70	142	0

Particle #	Particle Size (µm)	Two Populations (0 if only PE, 1 if PE and SE)
R71	357	0
R72	304	0
R73	386	0
R74	388	0
R75	476	0
R76	128	0
R77	310	0
R78	201	0
R79	583	0
R80	356	0
R81	316	0
R82	123	0
R83	132	0
R84	125	0
R85	308	0
R86	234	0
R87	268	0
R88	174	0
R89	420	0
R90	270	0
R91	337	0
R92	394	1
R93	227	0
R94	127	0
R95	172	0
R97	201	0
R98	136	0
R99	198	0
R100	276	0
R101	315	0
R102	391	0
R103	363	0
R104	261	0
R105	252	0
R106	418	0
R107	235	0
R108	209	0

Particle #	Particle Size (µm)	Two Populations (0 if only PE, 1 if PE and SE)
R109	388	0
R110	224	0
R111	282	1
R112	121	0
R113	134	0
R114	378	0
R115	258	0
R116	412	1
R117	366	0
R118	371	0
R119	207	0
R120	140	0
R121	173	0
R122	423	1
R123	136	0
R124	161	0
	SE Rating:	6.667

Spurr:

Particle #	Particle Size (µm)	Two Populations (0 if only PE, 1 if PE and SE)
S1(2)	445	0
S2	945	1
S3	562	0
S4	555	0
S5	641	1
S6	432	1
S7	381	1
S8	206	1
S9	206	0
S10	244	1
S11	254	0
S12	220	0

Particle #	Particle Size (µm)	Two Populations (0 if only PE, 1 if PE and SE)
S13	200	0
S15	302	1
S16	212	1
S17	150	1
S18	253	0
S19	230	0
S20	216	1
S21	244	1
S22	250	1
S23	210	1
S24	280	1
S25	293	1
S26	373	1
S27	182	1
S28	267	1
S29	187	1
S30	180	1
S31	230	1
S32	228	1
S33	232	1
S34	329	1
S35	255	1
S36	212	0
S37	286	1
S38	197	1
S39	253	1
S40	288	1
S41	270	1
S42	280	1
S43	190	1
S44	255	0
S45	243	0
S46	297	1
S47	239	1
S48	304	1
S49	213	0
S50	205	1

Particle #	Particle Size (µm)	Two Populations (0 if only PE, 1 if PE and SE)
S51	242	1
S52	306	1
S53	247	1
S54	336	1
S55	222	1
S56	326	0
S57	203	1
S58	190	1
S59	223	1
S60	170	0
S61	144	0
S63	198	1
S64	105	0
S65	242	0
S66	192	0
S67	178	0
S68	157	0
S69	177	1
S70	176	0
S71	226	1
S72	230	1
S73	229	0
S74	208	1
S75	152	0
S76	149	0
S77	236	0
S78	209	1
S79	183	0
S80	221	1
S81	250	0
S82	219	1
S83	195	1
S84	177	0
S86	206	1
S87	128	0
S88	172	0
S89	161	0

Particle #	Particle Size (µm)	Two Populations (0 if only PE, 1 if PE and SE)
S90	160	0
S91	189	0
S92	149	0
S93	184	0
S94	220	0
S95	198	1
S96	164	1
S97	131	0
S98	225	1
S99	175	1
S100	184	0
S101	193	0
S102	271	1
S103	172	1
S104	237	0
S105	239	1
S106	232	1
S107	185	1
S108	216	0
S109	200	0
S110	200	1
S111	277	1
S112	190	0
S113	228	1
S114	203	1
S115	244	1
S116	225	0
S117	164	1
S118	206	1
S119	169	0
S120	227	1
S121	244	0
S122	234	0
S123	183	1
S124	257	1
S125	172	1
S126	255	1

Particle #	Particle Size (µm)	Two Populations (0 if only PE, 1 if PE and SE)
S127	189	0
S128	202	1
S129	171	0
S130	288	0
S131	198	1
S132	243	1
	SE Rating:	60.465

Okmok:

Particle #	Particle Size (µm)	Two Populations (0 if only PE, 1 if PE and SE)
O1	238	1
O2	176	0
O3	134	0
O4	212	0
O5	264	0
O6	232	0
O7	201	0
O8	185	0
O9	215	1
O10	192	0
O11	286	1
O12	255	1
O13	281	1
O14	618	1
O15	382	1
O16	236	1
O17	308	1
O18	282	1
O19	312	1
O20	357	1
O21	323	0
O22	439	1

Particle #	Particle Size (µm)	Two Populations (0 if only PE, 1 if PE and SE)
O23	298	0
O24	323	1
O25	397	1
O26	321	1
O27	245	1
O28	323	1
O29	577	1
O30	190	1
O31	363	1
O32	417	0
O33	395	1
O34	525	0
O35	360	1
O36	506	1
O37	579	0
O38	450	1
O39	394	0
O40	315	1
O41	584	0
O42	607	1
O43	548	0
O44	336	0
O45	514	1
O46	419	1
O47	455	1
O48	358	0
O49	471	0
O50	575	1
O51	471	1
O52	1049	1
O53	236	1
O54	134	0
O55	284	0
O56	282	0
O57	232	0
O58	362	1
O59	250	0

Particle #	Particle Size (µm)	Two Populations (0 if only PE, 1 if PE and SE)
O60	708	1
O61	750	1
O62	269	0
O63	211	0
O64	688	0
O65	378	1
O66	507	1
O67	307	1
O68	246	0
O69	344	1
O70	310	0
O71	417	0
O72	629	0
O73	576	0
O74	311	1
O75	327	0
O76	260	0
O77	216	0
O78	341	0
O79	264	0
O80	330	1
O81	294	1
O82	348	0
O83	206	0
O84	250	1
O85	250	0
O86	194	1
O87	737	1
O88	272	1
O89	254	0
O90	351	0
O91	389	1
O92	514	1
O93	221	1
O94	294	0
O95	742	1
O96	446	1

Particle #	Particle Size (µm)	Two Populations (0 if only PE, 1 if PE and SE)
O97	155	1
O98	403	1
O99	185	1
O100	269	1
O101	302	0
O102	304	1
O103	240	0
O104	283	1
O105	345	1
O106	304	1
O107	259	1
O108	302	1
O109	288	1
O110	693	1
O111	378	0
O112	251	0
O113	270	1
O114	757	0
O115	266	0
O116	804	1
O117	630	1
O118	302	1
O119	291	1
O120	760	1
O121	352	1
O122	245	1
O123	328	1
O124	327	1
O125	206	1
O126	338	0
O127	354	1
O128	285	1
O129	350	1
	SE Rating:	61.240

Augustine:

Particle #	Particle Size (µm)	Two Populations (0 if only PE, 1 if PE and SE)
A1		1
A2(2)	323	1
A3(2)	461	1
A3(3)	464	1
A4(2)	380	0
A5(2)	409	1
A7(2)	540	1
A8(2)	198	1
A9	400	0
A10	265	1
A12	389	1
A13	320	0
A14	311	1
A15	221	0
A16	261	1
A17	225	1
A18	147	1
A19	341	1
A20	379	1
A21	323	1
A22	333	1
A23	341	1
A24	341	1
A25	400	1
A26	257	1
A27	395	0
A28	300	0
A29	165	1
A30	443	1
A31	310	1
A32	223	0
A33	202	1
A34	201	0
A35	322	0
A36	454	1

Particle #	Particle Size (µm)	Two Populations (0 if only PE, 1 if PE and SE)
A37	343	1
A38	276	0
A39	442	0
A40	416	1
A41	443	1
A42	383	1
A43	390	1
A44	416	1
A45	368	0
A46	690	1
A48	431	0
A49	371	1
A51	486	1
A52	420	1
A53	352	1
A54	510	1
A55	434	1
A56	184	0
A57	337	0
A58	307	1
A59	278	1
A60	254	0
A61	580	0
A62	218	1
A63	232	1
A64	442	0
A65	570	1
A67	346	0
A68	391	1
A69	676	1
A70	430	1
A71	483	0
A72	363	1
A73	411	0
A74	312	0
A75	679	1
A76	442	1

Particle #	Particle Size (µm)	Two Populations (0 if only PE, 1 if PE and SE)
A77	322	1
A78	345	1
A79	382	0
A80	400	0
A81	208	1
A82	334	0
A83	296	1
A84	436	1
A85	427	1
A86	259	0
A87	188	0
A88	235	0
A89	679	0
A90	344	1
A91	373	1
A92	281	0
A93	313	1
A94	274	1
A95	225	0
A96	247	0
A97	381	0
A98	275	1
A99	372	1
A100	430	1
A101	394	1
A102	362	1
A103	276	1
A104	317	0
A105	363	1
A106	169	0
A107	182	1
A108	330	1
A109	298	0
A110	260	1
A111	191	1
A112	232	1
A113	297	1

Particle #	Particle Size (µm)	Two Populations (0 if only PE, 1 if PE and SE)
A114	349	1
A115	234	0
A116	375	1
A117	260	1
A118	200	1
A119	358	1
A120	776	1
A121	263	1
A122	337	0
A123	273	0
A124	219	1
A125	335	1
A126	272	1
	SE Rating:	68.033

Saint Helens:

Particle #	Particle Size (µm)	Two Populations (0 if only PE, 1 if PE and SE)
MSH42	182	0
MSH43	186	1
MSH44	150	1
MSH45	218	1
MSH46	156	0
MSH47	133	1
MSH48	206	1
MSH49	152	0
MSH50	111	1
MSH51	147	0
MSH52	171	0
MSH53	111	0
MSH54	237	1
MSH55	156	1
MSH56	99.1	0

Particle #	Particle Size (µm)	Two Populations (0 if only PE, 1 if PE and SE)
MSH57	156	1
MSH58	286	0
MSH59	314	1
MSH60	279	1
MSH61	310	1
MSH62	412	1
MSH63	190	1
MSH64	296	0
MSH65	400	1
MSH66	194	1
MSH67	230	1
MSH68	286	1
MSH69	247	1
MSH70	373	1
MSH71	325	1
MSH72	305	1
MSH73	184	0
MSH74	265	0
MSH75	176	1
MSH76	170	1
MSH77	311	1
MSH78	193	0
MSH79	174	0
MSH80	161	0
MSH81	240	1
MSH82	257	0
MSH83	240	1
MSH84	260	0
MSH85	247	1
MSH86	254	1
MSH87	254	0
MSH88	267	1
MSH89	257	0
MSH90	366	1
MSH91	181	0
MSH92	320	1
MSH93	455	1

Particle #	Particle Size (µm)	Two Populations (0 if only PE, 1 if PE and SE)
MSH94	196	1
MSH95	278	1
MSH96	241	1
MSH97	216	1
MSH98	274	1
MSH99	236	0
MSH100	194	1
MSH101	243	1
MSH102	301	1
MSH103	257	1
MSH104	469	1
MSH105	336	0
MSH106	249	1
MSH107	340	0
MSH108	384	1
MSH109	340	1
MSH110	511	1
MSH111	360	1
MSH112	324	1
MSH113	339	1
MSH114	188	1
MSH115	249	1
MSH116	263	0
MSH117	188	1
MSH118	291	1
MSH119	313	1
MSH120	239	0
MSH121	219	1
MSH122	306	1
MSH123	282	0
MSH124	204	0
MSH125	241	1
MSH126	266	1
MSH127	260	1
MSH128	243	0
MSH129	301	1
MSH130	191	0

Particle #	Particle Size (µm)	Two Populations (0 if only PE, 1 if PE and SE)
MSH131	326	1
MSH132	244	0
MSH133	266	0
MSH134	261	1
MSh135	304	1
MSH136	335	1
MSH137	145	1
MSH138	307	0
MSH139	264	1
MSH140	210	0
MSH141	322	1
MSH142	341	1
MSH143	211	1
MSH144	232	1
MSH145	150	1
MSH146	247	0
MSH147	278	0
MSH148	285	1
MSH149	288	1
MSH150	272	1
MSH151	310	1
MSh152	335	1
MSH153	296	1
MSH154	157	1
MSH155	280	0
MSH156	293	1
MSH157	238	0
MSH158	275	1
MSH159	273	1
MSH160	246	0
MSH161	249	0
MSH162	236	1
MSH163	330	1
MSH164	243	1
MSH165	250	1
MSH166	173	0
MSH167	194	0

Particle #	Particle Size (µm)	Two Populations (0 if only PE, 1 if PE and SE)
MSH168	334	1
MSH169	396	1
MSH170	424	1
MSH171	221	0
MSH172	307	1
MSH173	229	1
MSH174	327	1
MSH175	215	0
	SE Rating:	68.657

Novarupta-Katmai:

Particle #	Particle Size (µm)	Two Populations (0 if only PE, 1 if PE and SE)
K1	508	0
K2	450	1
K3(2)	441	1
K4(2)	388	0
K5(2)	516	1
K6(2)	707	1
K7(2)	297	1
K8(2)	437	1
K9	348	1
K10	510	1
K11	635	1
K12	261	1
K13	281	1
K14	579	1
K15	475	1
K16	522	1
K17	307	1
K18	566	1
K19	453	1
K20	535	1

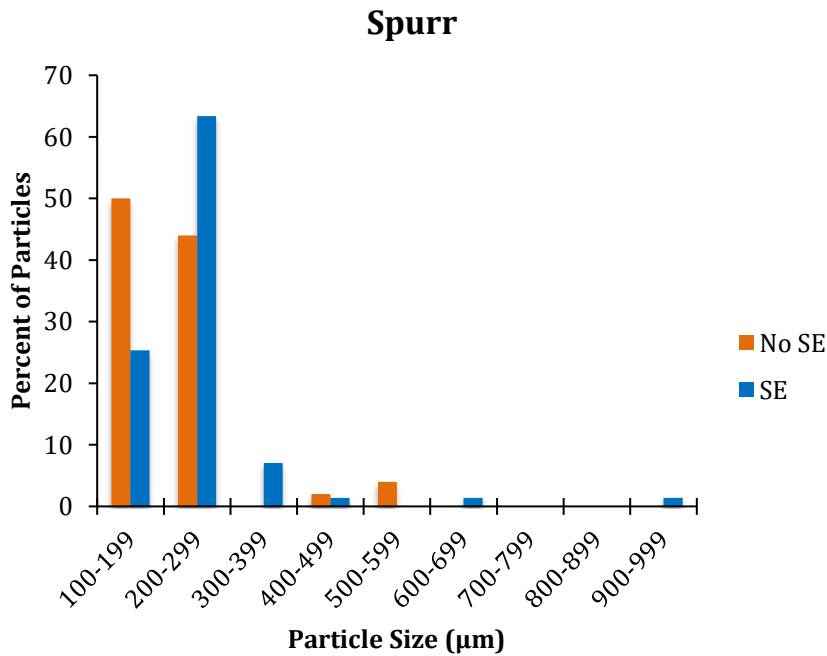
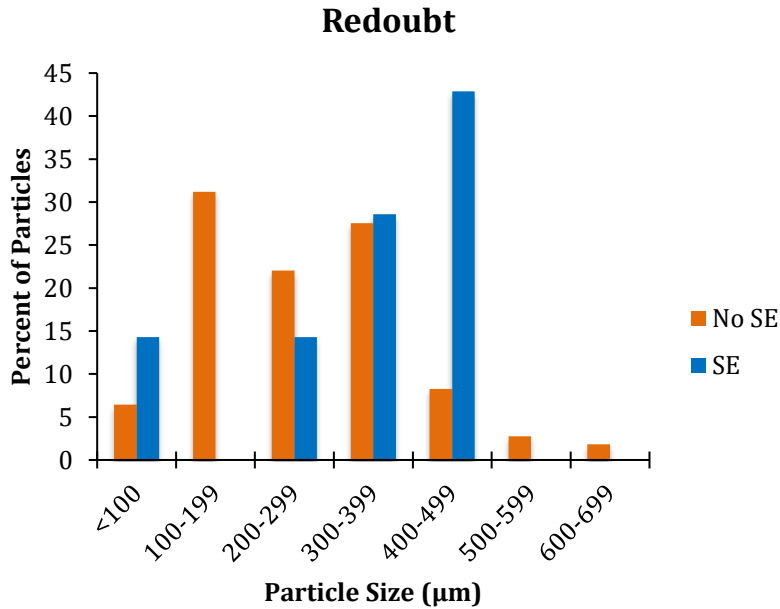
Particle #	Particle Size (µm)	Two Populations (0 if only PE, 1 if PE and SE)
K21	910	1
K22	425	1
K23	372	1
K24	374	1
K25	354	1
K26	410	1
K27	456	1
K28	425	1
K29	546	1
K30	365	1
K31	355	1
K32	289	1
K33	874	1
K34	690	0
K35	288	1
K36	269	1
K37	353	1
K38	455	1
K39	322	1
K40	606	1
K41	517	1
K42	563	0
K43	331	1
K44	291	1
K45	554	1
K46	462	1
K47	387	1
K48	554	1
K49	316	1
K50	380	1
K51	470	1
K52	512	1
K53	466	1
K54	223	1
K55	490	1
K56	685	0
K57	350	1

Particle #	Particle Size (µm)	Two Populations (0 if only PE, 1 if PE and SE)
K58	265	1
K59	543	1
K60	461	0
K61	626	1
K62	270	1
K63	436	0
K64	335	1
K65	452	1
K66	576	1
K67	645	1
K68	355	0
K69	346	1
K70	398	1
K71	401	1
K72	608	0
K73	855	1
K74	268	0
K75	391	0
K76	370	0
K77	394	0
K78	404	1
K79	325	1
K80	370	1
K81	412	1
K82	324	0
K83	373	0
K84	401	0
K85	273	0
K86	282	1
K87	275	1
K88	308	1
K89	288	1
K90	290	1
K91	231	0
K92	357	1
K93	334	1
K94	393	0

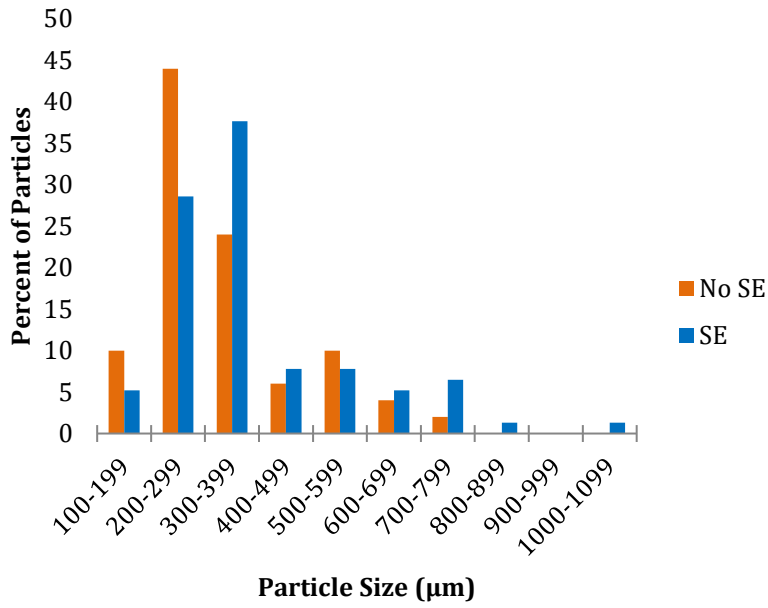
Particle #	Particle Size (µm)	Two Populations (0 if only PE, 1 if PE and SE)
K95	293	1
K96	277	1
K97	272	1
K98	314	0
K99	228	1
K100	391	0
K101	340	1
K102	381	1
K103	428	1
K104	345	1
K105	244	1
K106	297	0
K107	245	1
K108	323	1
K109	267	0
K110	411	1
K111	270	1
K112	363	1
K113	314	1
K115	363	1
K116	385	0
K117	430	1
K118	406	1
K119	329	1
K120	596	1
K121	353	1
K122	465	1
K123	505	1
K124	430	1
K125	367	0
K126	341	0
K127	684	1
K128	482	1
K129	596	0
K130	369	0
K131	307	1
K132	438	1

SE Rating:	78.6259542

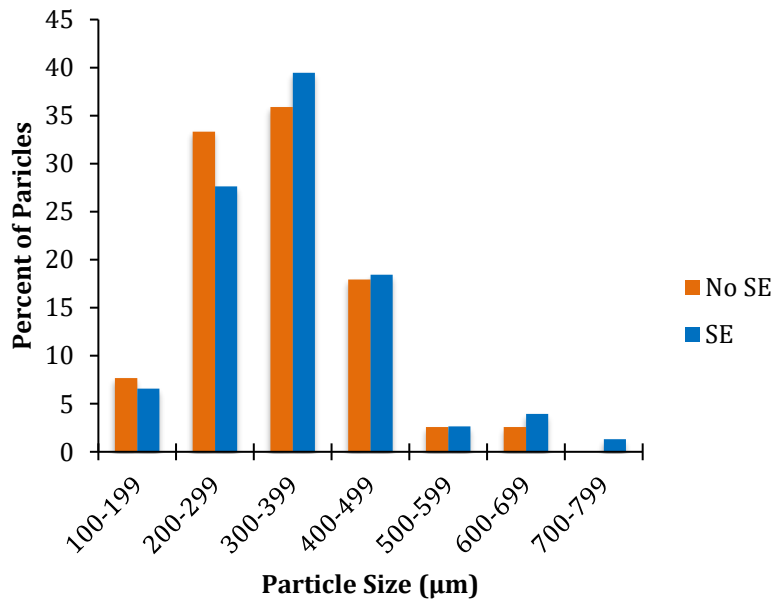
Appendix 2: Particle size distributions from each eruption, differentiating between particles with syn-eruptive bubbles (SE) and particles with no syn-eruptive bubbles (No SE). There is not clear correlation between particle size and the likelihood of preserving or not preserving syn-eruptive bubbles.

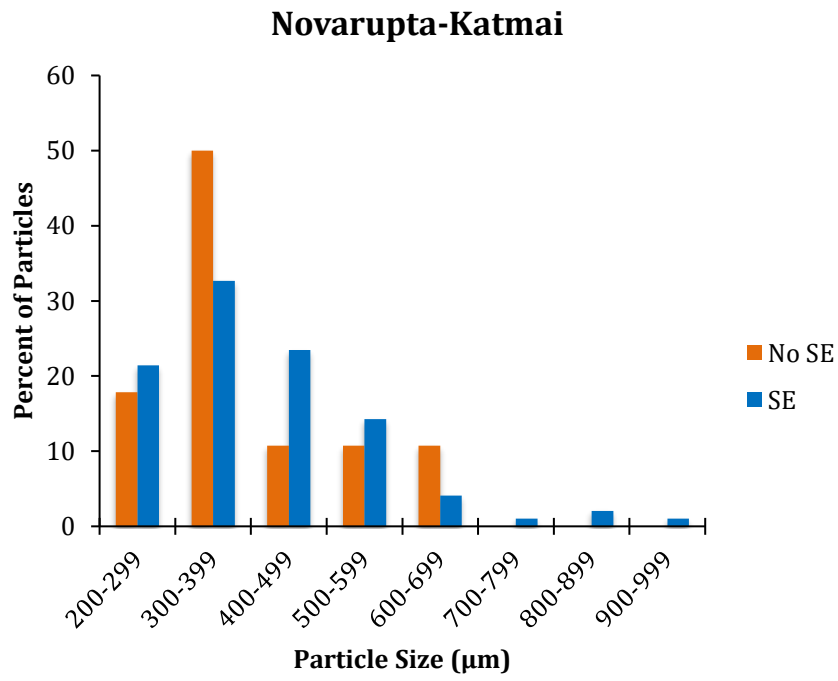
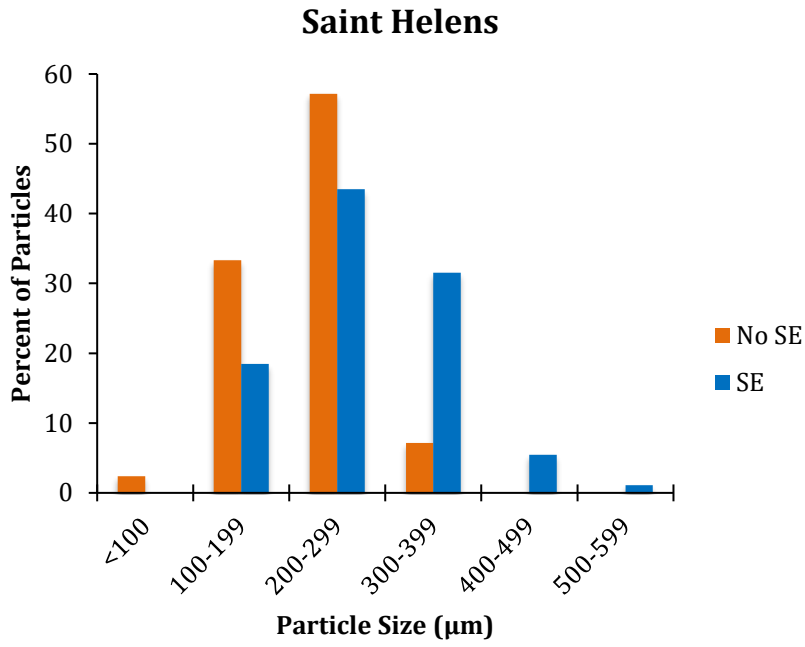


Okmok



Augustine





VITA

Megan Clark is from Syracuse, NY. Her parents are Thomas and Deborah Clark. She graduated with honors from the George Washington University in 2015 with a BA in Geological Sciences and Environmental Studies. At GWU, she was a Presidential Scholar, member of the University Honors Program, and recipient of the George C. Stevens Geological Sciences Award. She will graduate in May 2017 from Lehigh University with her MS in Earth and Environmental Sciences. At Lehigh, she was nominated for the University Teaching Assistant Award and won Best Poster at the 2017 EES Graduate Symposium.